Water Resources Research

RESEARCH ARTICLE
10.1029/2021WR029753

Quantifying Dam-Induced Fluctuations in Streamflow Frequencies Across the Colorado River Basin

Jeongwoo Hwang[1], Hemant Kumar[2], Albert Ruhi[3], Arumugam Sankarasubramanian[2], and Naresh Devineni[1]

[1]Department of Civil Engineering, The City University of New York (City College), New York, NY, USA, [2]Department of Civil, Construction, and Environmental Engineering, North Carolina State University, Raleigh, NC, USA, [3]Department of Environmental Science, Policy, and Management, University of California, Berkeley, Berkeley, CA, USA

Key Points:

- Temporal changes in streamflow frequency are explored in the Colorado River Basin
- Magnitude of frequency alteration changes with annual frequencies recovering and multi-annual remaining altered across the river network
- Dams that significantly alter streamflow frequencies exist across the entire network, and more so in the Lower Colorado Basin

Supporting Information:

Supporting Information may be found in the online version of this article.

Correspondence to:

J. Hwang,
jhwang1@ccny.cuny.edu

Citation:

Hwang, J., Kumar, H., Ruhi, A., Sankarasubramanian, A., & Devineni, N. (2021). Quantifying dam-induced fluctuations in streamflow frequencies across the Colorado River Basin. *Water Resources Research*, *57*, e2021WR029753. https://doi.org/10.1029/2021WR029753

Received 7 FEB 2021
Accepted 2 OCT 2021

Abstract Periodic fluctuations in natural streamflow are a major driver of river ecosystem dynamics and water resource management. However, most U.S. rivers are impacted both by long-term hydroclimatic trends and dams that alter flow variability. Despite these impacts, it remains largely unexplored how dams affect the dominant frequencies of natural streamflow over a highly regulated river network. We investigated the entire Colorado River Basin (CRB) to understand how the annual (10–14 months) and multi-annual (24–60 months) frequencies in natural flow regimes have been progressively altered by dams. Given the significant alteration over the CRB, we captured changes in streamflow frequencies between naturalized and observed monthly flows via wavelet analysis. Based on the similarity of changes in streamflow frequencies (annual and multi-annual) over the last 30 years, sections of the riverine network were classified into four groups. The annual frequency was relatively well preserved downstream of Hoover Dam, while showing a systematic trend of alteration downstream of Glen Canyon Dam until Hoover Dam. Meanwhile, the multi-annual frequency component was highly altered for the entire Lower Colorado main stem (i.e., downstream of Glen Canyon). We also identified dams with significant impacts on streamflow frequency by comparing wavelet coherence estimates. This study advances the notion that dams fundamentally alter river flow regimes across multiple frequencies and with varying amplitudes over time and space, with alteration propagating – or being dampened – by both hydroclimatic fluctuations and water resource management.

1. Introduction

As water demand drastically increased due to growing population and urbanization over the last century, a vast installation of reservoirs proliferated worldwide, fundamentally changing the water cycle (Ripl, 2003). Large-scale water regulation and conveyance systems currently determine present and future water availability to society (Sivapalan et al., 2003, Vogel et al., 2015; Vörösmarty & Sahagian, 2000). In the United States (U.S.) alone, more than 90,000 dams change the quantity and variability of natural flow regimes, altering an estimated >85% of inland waterways (National Research Council, 1992). The impacts of such alteration propagate through river networks and affect the fluvial ecosystem in multiple ways: by preventing sediment transport (Willis & Griggs, 2003), by stabilizing channel morphology (Brandt, 2000; Graf, 2006; Topping et al., 2000), by fundamentally changing thermal and flow regimes (Olden & Naiman, 2010; Poff et al., 2007; Ruhi et al., 2019), and by altering the composition and dynamics of aquatic biota (Bunn & Arthington, 2002; Poff et al., 2007).

Many studies have investigated dam-induced flow alteration, mostly by estimating the proportion of annual flows that can be withheld by a dam or a cluster of dams (Graf, 1999; Grill et al., 2014, 2015; Lehner et al., 2011; Mailhot et al., 2018; Nilsson et al., 2005; Vörösmarty & Sahagian, 2000). However, this metric may not capture whether flow alteration is affecting the periodic ('signal') or stochastic ('noise') components of streamflow. Streamflow periodicity is a critical element in water supply and hydropower generation planning (Koch et al., 2011), and for riparian and aquatic biota with life histories that are 'coupled' with cyclical, predictable high and low flows (Lytle & Poff, 2004). Additionally, previous studies have largely provided a single, time-invariant estimate that averages fluctuations in alteration in trying to understand how both climate and dams together alter the flow regime (Chalise et al., 2021). Because dam operations change over time with dam specific objectives and regional climatic conditions, there is increasing recognition that

time-invariant metrics may not be sufficient to explain streamflow alteration and its impacts (Poff, 2018; Ruhi et al., 2018). Developing time-varying flow alteration metrics may help better understand the transience of hydrologic conditions in river basins dominated by dams – as well as their impacts. In addition, showing the local and watershed-scale spatiotemporal variability of streamflow alteration, which shapes biota and ecosystem processes along river networks, could help prioritize selection of sites for restoration (Palmer & Ruhi, 2019).

Streamflow variability has been typically expressed in the time domain (Box & Jenkins, 1970; Gao et al., 2009; Thomas & Fiering, 1962), and more recently also in the frequency domain (Milly & Wetherald, 2002; Patskoski et al., 2015). Wavelet transforms, which permit the orthogonal decomposition of a time series into both time and frequency domains, have been applied to many geophysical time series (Farge, 1992; Foufoula-Georgiou & Kumar 2014; Hubbard, 1996; Kulkarni, 2000; Kwon et al., 2006, 2007; Wang & Wang, 1996; Weng & Lau, 1994). Some studies have demonstrated the usefulness of wavelet analysis for assessing post-dam operational discharge modulations at specific frequencies (Ruhi et al., 2018; White et al., 2005). Wavelet analysis provides information on the frequency at all scales and times with a single spectrum image that is easy to interpret, can be used when management history is uncertain, and performs well even if the underlying data (e.g., streamflow) is non-stationary due to external forcing (e.g., climate change) or local management. Building on the univariate wavelet transform, wavelet coherence examines the relationship of two time series in the time-frequency domain (Grinsted et al., 2004; Torrence & Compo, 1998), making it an ideal tool to assess how time-varying flow alteration may propagate across a river network.

Here we performed wavelet coherence analysis based on the wavelet transforms of controlled (observed) and naturalized (modeled "free-flowing") streamflow data. This analysis allowed us to explore the degree of alteration in streamflow over time – focusing on its annual and multi-annual frequencies. The Colorado River Basin, a highly regulated fluvial network, is used for demonstration purposes. Similarities in the degree of alteration across the basin were quantified using the dynamic time warping clustering method (Berndt & Clifford, 1994; Keogh & Ratanamahatana, 2005). Loss of wavelet coherence represents the cumulative alteration of streamflow due to both climate and human activities. Controlled flows result from regional climate forcing, basin characteristics, and anthropogenic factors. In contrast, naturalized flows were derived by removing the anthropogenic factors. Wavelet coherence between the two (natural and controlled flows) measures the local correlation in the time-frequency space, revealing locally phase-locked behavior (Grinsted et al., 2004). Whereas high coherence at a given frequency and time indicates little to no alteration, low coherence suggests high alteration. As we quantified the degree of alteration, we also identified dams with significant impacts on local and basin-wide alteration. We primarily focused on the annual and multi-annual frequencies since streamflow seasonality (i.e., the cycle of high and low flows) has a regular annual periodicity, while large-scale climatic fluctuations tend to manifest at a multi-annual scale. We also identified dams with significant impacts on their local streamflow frequency and discuss the significance of our approach to quantify time-varying flow alteration in the frequency domain and its propagation across a river network.

2. Data

2.1. The Colorado River Basin and Its Importance for Water Management

We focused on the Colorado River Basin (CRB) owing to its high levels of regulation, data availability, and importance for water resources management in the United States. Starting from Wyoming and Colorado, the Colorado River flows for about 2,300 km until it crosses the international border with Mexico (Figure 1). The total drainage area is about 637,000 km^2, and extends over seven U.S. states: Arizona, California, Colorado, New Mexico, Nevada, Utah, and Wyoming. More than 25 million people and ~12,000 km^2 of cropland depend on the Colorado River for water supply (Bruce, 2012). Colorado River water is partially diverted to serve Denver, Salt Lake Valley, Albuquerque, Cheyenne, Los Angeles, San Diego, and Imperial Valley in California. The CRB is commonly divided into two parts, the Upper (UCRB) and the Lower Colorado River Basin (LCRB), located upstream and downstream of Lees Ferry (immediately downstream of Glen Canyon Dam), respectively. The UCRB includes most of the headwaters of the Colorado River, while the LCRB comprises the strongly regulated and heavily altered downstream section. More than 1,400 dams exist in this basin, including the Hoover Dam and Glen Canyon Dam, which create the two largest reservoirs in the U.S.

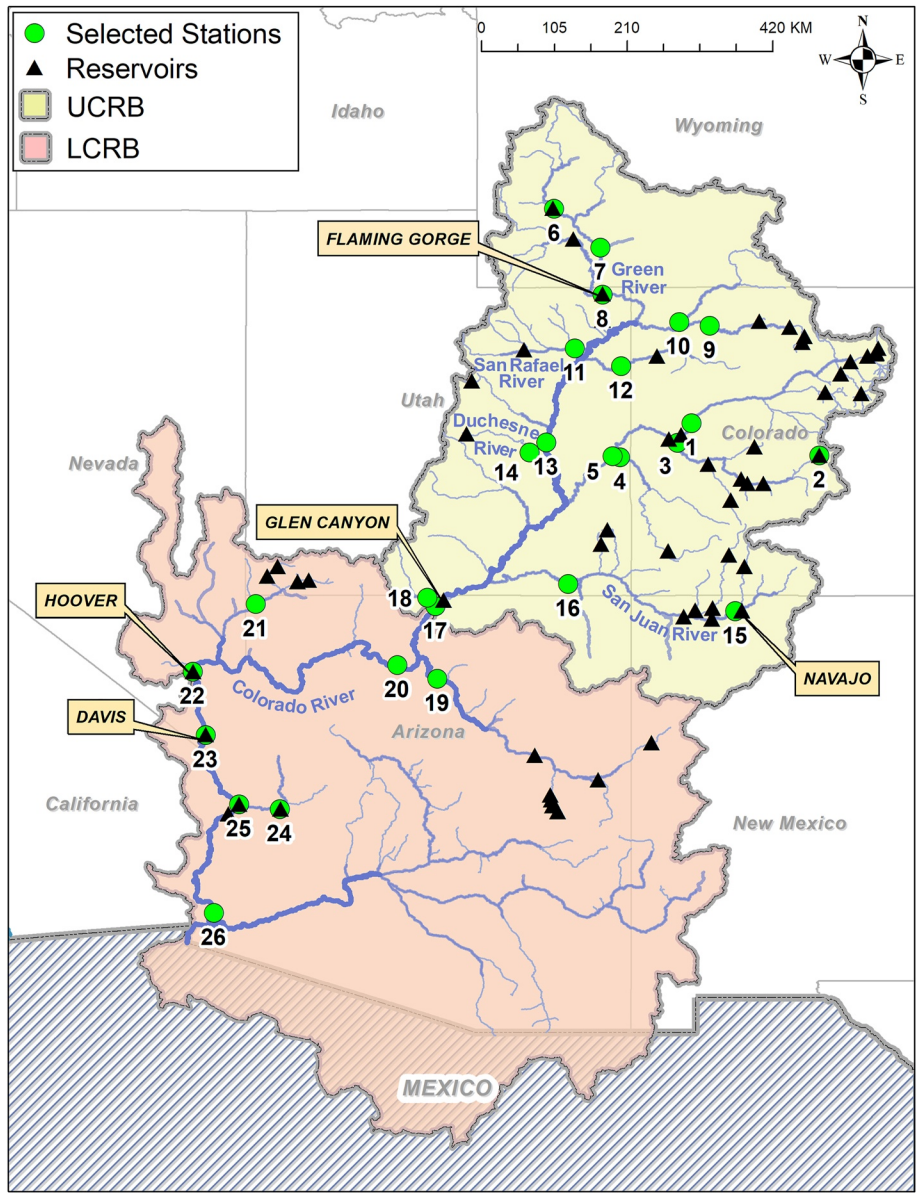

Figure 1. Spatial distribution of the 26 selected USGS streamflow gauging stations and 61 intermediate-to-large NID dams across the Colorado River Basin (including both Upper and Lower Colorado Basins). Station numbers are also presented.

by volume (U.S. Army Corps of Engineers, 2020). Glen Canyon Dam and Hoover Dam have been operating since 1963 and 1936, respectively, altering flow regimes along the Colorado River due to operations at various time scales – sub-daily hydropeaking, seasonal low flow augmentation and flood control, and long-term inter-basin transfers (Maupin et al., 2018; U.S. Department of the Interior and Office of the Secretary of the Interior, 1996; Wiele & Smith, 1996).

Historical observations of precipitation in the CRB show strong annual and decadal variabilities that are assumed to be associated with global climate processes, such as El Niño-Southern Oscillation (ENSO) and Pacific Decadal Oscillation (PDO) (Kalra & Ahmad, 2012; Nowak et al., 2012; Redmond & Koch, 1991; Ropelewski & Halpert, 1986; Tamaddun et al., 2017). Several studies have shown that the southwestern U.S. often receives above-normal (below-normal) precipitation during strong El Niño (La Niña) years (Hidalgo & Dracup, 2003; Ropelewski & Halpert, 1986; Webb & Betancourt, 1992). Nevertheless, the UCRB and LCRB show distinctly different hydroclimatic characteristics. Monthly precipitation in the UCRB shows

a relatively even distribution throughout the year, while precipitation over the LCRB generally shows significant seasonality with a sharp peak in summer and a secondary peak in winter (Sheppard et al., 2002; Whitlock & Bartlein, 1993). Snowmelt water from the Rocky Mountains contribute ~70% of the UCRB's annual streamflow (Christensen et al., 2004). That is, streamflow variations during the warm season (April–September) in the UCRB are heavily dependent on snowpacks, which are determined by precipitation during the antecedent cold season (October–March). The hydroclimatology of LCRB is characterized by quick storm events and flash floods associated with the North American Monsoon, especially during the warm season (Douglas et al., 1993; Higgins et al., 1999).

2.2. Naturalized Flow Data

Monthly time series of naturalized streamflow developed by the United States Bureau of Reclamation are available for 26 streamflow sites over the CRB. Historical data of monthly consumptive uses and losses, reservoir regulations, and historic flow in CRB were taken into account to calculate naturalized streamflow (Prairie & Callejo, 2005). Monthly consumptive uses and losses in the UCRB were obtained at a USGS hydrologic unit code (HUC) based on Consumptive Uses and Losses Reports, which have been published every five years since 1971. For the LCRB, Decree Accounting records of water use were utilized to determine consumptive uses and losses. The historic reservoir regulation data accounts for water storage and release from 12 mainstem reservoirs and 25 off-stream reservoirs located within the basin. The resultant naturalized flow covers 111 years ranging from 1906 to 2016, at a monthly scale.

2.3. Observed Flow Data

At the 26 USGS streamflow gauging stations with available naturalized streamflow, monthly streamflow records have been continuously reported for at least 30 years between 1906 and 2016. The corresponding observed monthly streamflow data were retrieved from the USGS National Water Information System (NWIS), with period of record varying by station (average length of 79 years) and the common period of record beginning in 1987. As this study intended to explore the level of streamflow alteration relative to its natural state, a wavelet coherence analysis between naturalized and observed streamflow (both at the monthly time scale) was carried out for the time span where continuous data is available, including the common period (1987–2016), at each station. The spatial distribution of the selected USGS gauging stations is shown in Figure 1. Stations are indexed, listed, and georeferenced in Table 1. Standardized time series of observed and naturalized flows at each 26 selected USGS streamflow gauging stations are provided in Figure S1 in Supporting Information S1.

2.4. Criteria for Dam Selection

According to the National Inventory of Dams (NID) database, 1,455 dams are present in the CRB, fulfilling various purposes (mainly hydropower, flood control, water supply and irrigation). Here we only considered intermediate to large dams, i.e., those with a height greater than 12.2 meters or a storage capacity over 1.23 million m^3, following the definition of the American Society of Civil Engineering (Snyder, 1964). This procedure returned 61 dams (Figure 1), which are assumed to impact the riverine system where the 26 streamflow gauges are located. Most of these selected dams were constructed before 1987, and their cumulative capacity is >99.9% of the total storage of the 61 dams. We therefore assumed that further dam construction post-1987 had lesser impacts on flow regime alteration (e.g., via increased capacity). Connectivity between the selected dams and streamflow gauges was developed based on the River and Infrastructure Connectivity Network (RICON) tool, which systematically combines three geospatial information sources: the National Hydrographic Dataset (NHDPlusV2), streamflow gauges from the USGS National Water Information System, and NID reservoirs (Mukhopadhyay et al., 2020).

Table 1
Details of the USGS Streamflow Gauging Stations Used in the Study

Index number	NWIS site number	NWIS site name (description of location)	Drainage area (km^2)	Elevation (km)	Controlled flow data availability
1	9,095,500	COLORADO RIVER NEAR CAMEO, CO.	20,683	1.47	1933.10–2016.12
2	9,109,000	TAYLOR RIVER BELOW TAYLOR PARK RESERVOIR, CO.	657	2.80	1938.10–2016.12
3	9,152,500	GUNNISON RIVER NEAR GRAND JUNCTION, CO.	20,520	1.41	1916.10–2016.12
4	9,180,000	DOLORES RIVER NEAR CISCO, UT	11,862	1.27	1986.10–2016.12
5	9,180,500	COLORADO RIVER NEAR CISCO, UT	62,418	1.25	1922.10–2016.12
6	9,211,200	GREEN RIVER BELOW FONTENELLE RESERVOIR, WY	11,085	1.94	1963.12–2016.12
7	9,217,000	GREEN RIVER NEAR GREEN RIVER, WY	36,259	1.85	1951.10–2016.12
8	9,234,500	GREEN RIVER NEAR GREENDALE, UT	50,245	1.71	1963.10–2016.12
9	9,251,000	YAMPA RIVER NEAR MAYBELL, CO	8,761	1.80	1916.05–2016.12
10	9,260,000	LITTLE SNAKE RIVER NEAR LILY, CO	10,448	1.73	1921.10–2016.12
11	9,302,000	DUCHESNE RIVER NEAR RANDLETT, UT	9,816	1.45	1942.10–2016.12
12	9,306,500	WHITE RIVER NEAR WATSON, UT	10,411	1.51	1923.10–2016.12
13	9,315,000	GREEN RIVER AT GREEN RIVER, UT	116,160	1.23	1905.03–2016.12
14	9,328,500	SAN RAFAEL RIVER NEAR GREEN RIVER, UT	4,216	1.28	1945.10–2016.12
15	9,355,500	SAN JUAN RIVER NEAR ARCHULETA, NM	8,443	1.72	1962.10–2016.12
16	9,379,500	SAN JUAN RIVER NEAR BLUFF, UT	59,569	1.23	1927.04–2016.12
17	9,380,000	COLORADO RIVER AT LEES FERRY, AZ	289,560	0.94	1921.10–2016.12
18	9,382,000	PARIA RIVER AT LEES FERRY, AZ	3,651	0.95	1923.10–2016.12
19	9,402,000	LITTLE COLORADO RIVER NEAR CAMERON, AZ	68,528	1.21	1947.10–2016.12
20	9,402,500	COLORADO RIVER NEAR GRAND CANYON, AZ	366,742	0.74	1922.10–2016.12
21	9,415,000	VIRGIN RV AT LITTLEFIELD, AZ	13,183	0.54	1929.10–2016.12
22	9,421,500	COLORADO RV BLW HOOVER DAM, AZ-NV	444,700	0.21	1934.04–2016.12
23	9,423,000	COLORADO RIVER BELOW DAVIS DAM, AZ-NV	448,844	0.15	1949.03–2016.12
24	9,426,000	BILL WILLIAMS RIVER BELOW ALAMO DAM, AZ	11,999	0.30	1969.10–2016.12
25	9,427,520	COLORADO RIVER BELOW PARKER DAM, AZ-CA	473,190	0.09	1935.01–2016.12
26	9,429,490	COLORADO RIVER ABOVE IMPERIAL DAM, AZ-CA	488,212	NA	1976.10–2016.12

3. Methods

We took both the naturalized and controlled streamflow series for each station and computed the wavelet coherence spectrum between them – delivering a localized coefficient for each of the 256 frequency scales over the given period. Further details on the wavelet coherence analysis are discussed in Section 3.2. The wavelet coherence spectrum between the 10-month and 14-month frequency scales was then selected and averaged (across scales) into the annual frequency band for each timestep. Similarly, for the multi-annual frequency band, the wavelet coherence spectrum for frequency scales between the 24- and 60-months was selected and scale-averaged for each timestep. The scale-averaged wavelet coherence loss for each frequency band was then computed by subtracting the wavelet coherence value from 1. This scale-averaged wavelet coherence loss time series measures the degree of alteration over time. We finally grouped stations with similar time-varying wavelet coherence loss for each frequency band using the dynamic time warping hierarchical clustering method.

In the following sub-sections, we provide details on the wavelet transform, wavelet coherence, and dynamic time warping hierarchical clustering methods. In Figure 2, we present the workflow diagram for the systematic approach that was carried out in this study.

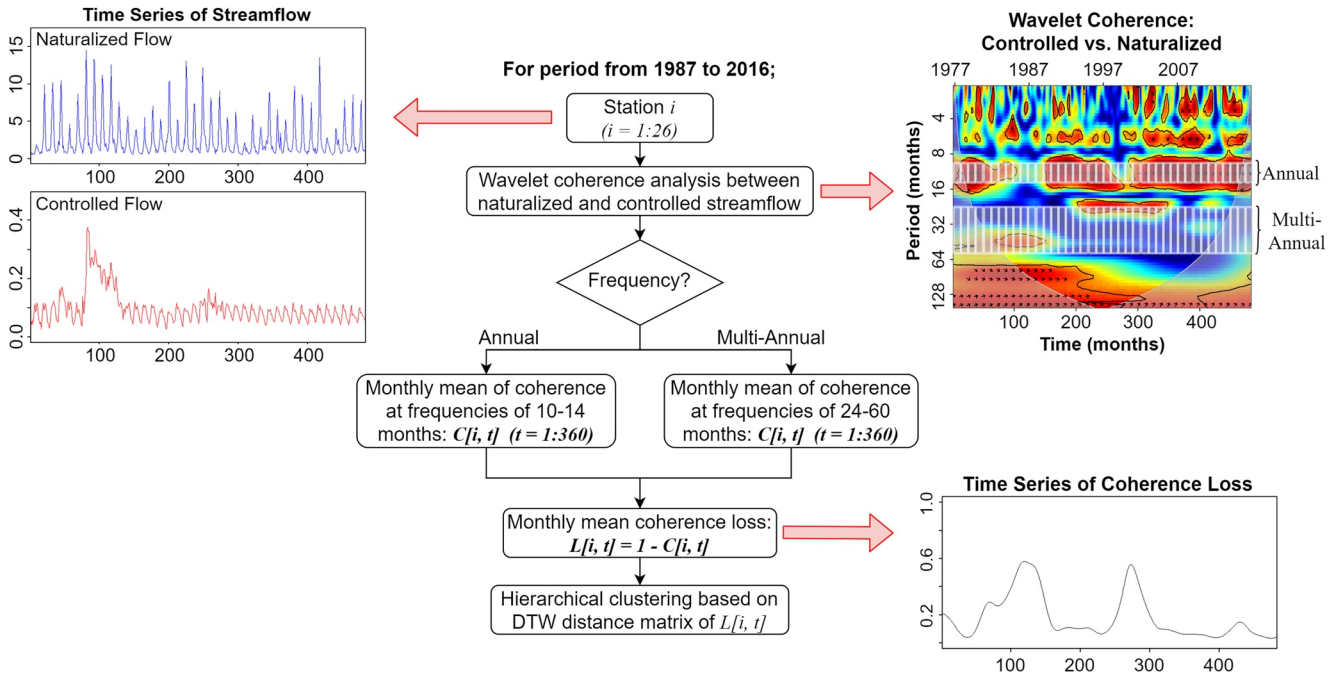

Figure 2. Methodological flowchart for the wavelet coherence analysis.

3.1. Wavelet Transform

As this study investigated the level of alteration in streamflow relative to its natural state in terms of time and frequency, we determined wavelet coherence between monthly naturalized and controlled (observed) streamflow. Decomposing a time series into a time-frequency domain allows for localizing intermittent periodicities across scales (Torrence & Compo, 1998). This process conjugates the given time series with a flexible wavelet function, which can be temporally dilated/compressed while it translates along the time-steps. High-frequency features of a given time series can be captured with a wavelet function narrow in time, whereas low-frequency components can be analyzed with a dilated wavelet function. A variety of wavelet functions (or 'mother wavelets') are available; here, we implemented the Morlet wavelet, defined as,

$$\psi_0(\eta) = \pi^{-1/4} e^{iw_0\eta} e^{-\eta^2/2} \tag{1}$$

where w_0 and η are the dimensionless frequency and time, respectively. The non-dimensional frequency of the Morlet wavelet was set as 6 in this study to satisfy the wavelet admissibility (Farge, 1992). This complex wavelet function returns information about both the amplitude and phase, and thus makes itself applicable for describing wave-like oscillatory behaviors such as streamflow and precipitation (Kumar & Foufoula-Georgiou, 1997; Labat, 2005; Torrence & Compo, 1998). The continuous wavelet transform of a discrete time series (x_n) with equal time spacing of δt is defined as the convolution with a scaled and normalized wavelet function (Torrence & Compo, 1998) as

$$W_b^X(a) = \sum_{n=0}^{N-1} x_n \psi^* \left[(n-b) \frac{\delta t}{a} \right] \tag{2}$$

where $W_b^X(a)$ is the wavelet spectrum, a is the scale parameter, b is the localized time index, N is the total number of sample points in the time series, the (*) indicates complex conjugate, and ψ is the normalized ψ_0. The ψ_0 was normalized to have unit energy at each scale in Equation 2 to ensure the wavelet transforms at each scale are directly comparable. The convolution was done for N times for each scale to estimate the wavelet power spectrum in both time and frequency scales, and the wavelet power is defined as $\left|W_b^X(a)\right|^2$.

3.2. Wavelet Coherence

Wavelet coherence is a quantity that describes the coherence between two different time series based on their cross-wavelet transforms as a function of both time and frequency. Given two time series X and Y, the cross-wavelet spectrum is defined as

$$W_b^{XY}(a) = W_b^X(a) W_b^{Y*}(a) \tag{3}$$

where (*) denotes the complex conjugate. The cross-wavelet spectrum reveals the covariance between the time series as a function of time and frequency. By dividing the square of the absolute value of the smoothed cross-wavelet power with smoothed wavelet power spectra, one can obtain the wavelet coherence, R^2 (Torrence & Webster, 1999):

$$R^2 = \frac{\left|\langle a^{-1} W_b^{XY}(a)\rangle\right|^2}{\langle a^{-1}\left|W_b^X(a)\right|^2\rangle \cdot \langle a^{-1}\left|W_b^Y(a)\right|^2\rangle} \tag{4}$$

This provides a quantity ranging from 0 to 1, representing the localized correlation coefficient in time and frequency space (Grinsted et al., 2004). The brackets $\langle\cdot\rangle$ in Equation 4 indicate smoothing in both time and scale. For the Morlet wavelet, the temporal smoothing operator is a Gaussian function, $e^{-t^2/\left(2s^2\right)}$, while the scale smoothing is done using a boxcar filter. For a more elaborate description of the wavelet coherence, see Torrence and Webster (1999).

We were interested in knowing how wavelet coherence between the naturalized and controlled flow evolved over time at the annual and multi-annual frequency bands. To this end, we computed the scale-averaged coherence for each time step based on each frequency band of the annual frequency (10–14 months) and multi-annual frequency (24–60 months). In turn, the coherence loss at each timestep was calculated by subtracting the coherence value from 1. This procedure yields a time series of wavelet coherence loss of controlled relative to naturalized flow at the annual and multi-annual frequency bands. Sub-annual frequencies were not examined in this study since these are primarily associated with short-term management, which may produce high-frequency signals that are difficult to differentiate from random noise. Moreover, we assumed these short-term management signals would have a low impact on the systematic coherence loss in streamflow across the basin. We note that the resolution of a continuous wavelet transform is determined by the tradeoff between temporal and frequency resolutions of the wavelet. We can retain the temporal accuracy of the scale-averaged wavelet coherence loss in the annual frequency scale, whereas loss in the multi-annual frequency scale contains less accurate temporal information. Thus, for multi-annual features we focus on long-term trends rather than explaining them locally. While we focused on annual and multi-annual frequency resolutions because the given data were at the monthly time scale, if daily/sub-daily data are available, sub-daily management signals could be also resolved. For example, Ciria et al. (2019) identified streamflow regime breakpoints caused by anthropogenic factors at different scales, including sub-weekly, weekly, and annual scales, using wavelet analysis.

3.3. Dynamic Time Warping Based Hierarchical Clustering

To explain the regional discordance between controlled and naturalized flow across the basin, stations were clustered in groups based on their scale-averaged time-varying wavelet coherence loss from 1987 to 2016. Since most dams in the basin were constructed before 1987, coherence analysis after this period provides a complete dam-induced alteration signal. Euclidean distance is typically used as a similarity measure for clustering. However, as Euclidean distance is determined by aligning the *ith* point in one sequence with the *ith* point in the other, it is susceptible to phase lags and outliers, a critical aspect when clustering cascading stations. Here we implemented the dynamic time warping (DTW) technique instead, which provides a robust distance metric for similarity quantification. Unlike the Euclidean distance, DTW is a flexible measure that can detect similarities between time series even if they are out of phase (Berndt & Clifford, 1994; Keogh & Ratanamahatana, 2005). Based on the DTW similarity measures, the wavelet coherence loss dynamics at different stations were grouped using the hierarchical clustering method. The optimal number of clusters

Table 2
Summary of Wavelet Coherence Simulation

Frequency band	Wave component	Simulation	Description
Annual	Amplitude	$A_1 = 1$ (Constant)	Significant change in wavelet coherence is observed only when the amplitude was completely diminished
		$A_3 = 1, \frac{2}{3}, \frac{1}{3}, 0$	
	Phase Lag	$\varphi_1 = 0$ (Constant)	Wavelet coherence instantaneously fluctuates whenever the phase lag changes by π
		$\varphi_3 = 0, \frac{\pi}{4}, \frac{\pi}{2}, \pi, 0$	
	Frequency	$f_1 = 12$ (Constant)	A permanent shift in the wavelet coherence is observed whenever there is a change in the frequency
		$f_3 = 12, 13, 15, 17$	
Multi-Annual	Amplitude	$A_2 = 1$ (Constant)	Significant change in wavelet coherence is observed only when the amplitude was completely diminished
		$A_4 = 1, \frac{2}{3}, \frac{1}{3}, 0$	
	Phase Lag	$\varphi_2 = 0$ (Constant)	Wavelet coherence instantaneously fluctuates whenever the phase lag changes by π
		$\varphi_4 = 0, \frac{\pi}{4}, \frac{\pi}{2}, \pi, 0$	
	Frequency	$f_2 = 48$ (Constant)	A permanent shift in the wavelet coherence is observed whenever there is a change in the frequency
		$f_4 = 48, 49, 54, 60$	

was determined based on the elbow method (Thorndike, 1953). The impacts of anthropogenic regulation and climatic forcing on wavelet coherence loss were then explored based on the resultant clusters.

3.4. Wavelet Coherence Interpretation Under "Known" Signals

Before interpreting wavelet coherence loss results for the CRB, we performed wavelet coherence under known time series signals, here referred to as "experiments". These experiments provide the sensitivity of wavelet coherence to changes in the wave components of signals in specific frequency bands. For this purpose, we created two noiseless identical sinusoidal time series (y_1 and y_2) containing both annual and multi-annual frequency signals (Equations 5 and 6):

$$y_1 = A_1 sin\left(2\pi f_1 t + \varphi_1\right) + A_2 sin\left(2\pi f_2 t + \varphi_2\right) \quad (5)$$

$$y2 = A_3 sin\left(2\pi f_3 t + \varphi_3\right) + A_4 sin\left(2\pi f_4 t + \varphi_4\right) \quad (6)$$

In the above equations, A_1 and A_3 are the amplitude of the annual signal; A_2 and A_4 indicate the amplitude of the multi-annual signal. f_1 and f_3 signify the annual frequency; f_2 and f_4 are the multi-annual frequency. φ_1 and φ_3 are the phase lag of the annual signal; and φ_2 and φ_4 represent the phase lag of the multi-annual signal. In a sequence of six simulations, one of the two time series, y_1, remains unperturbed, whereas the other, y_2, is set to have the signal characteristics change over time. Each simulation focused on one frequency band at a time, and measured wavelet coherence between the two time series while ensuring only one wave component changes over time. For example, in the first simulation, the amplitude of the second time series that relates to the annual frequency (A_3) is altered three times over the 1,500 time periods. Between $t = 1$ to $t = 375$, $A_3 = 1$; between $t = 376$ to $t = 750$, $A_3 = 2 / 3$; between $t = 751$ to $t = 1125$, $A_3 = 1 / 3$; and between $t = 1126$ to $t = 1500$, $A_3 = 0$; hence creating a time series where the amplitude systematically tapers off to zero. Likewise, in the second and third simulation, the phase lag (φ_3) and the frequency (f_3) is altered systematically. The amplitude (A_4), phase lag (φ_4) and frequency (f_4) of the multi-annual band were altered in simulations four to six. Phase lag components were altered four times over the 1,500 time periods during the simulations. Details of the six simulations are summarized in Table 2.

For both frequency bands, changes in the amplitude resulted in a temporary drop in the wavelet coherence, followed by an immediate recovery (Figures 3a and 3d). Unless the amplitude of the frequency signal was

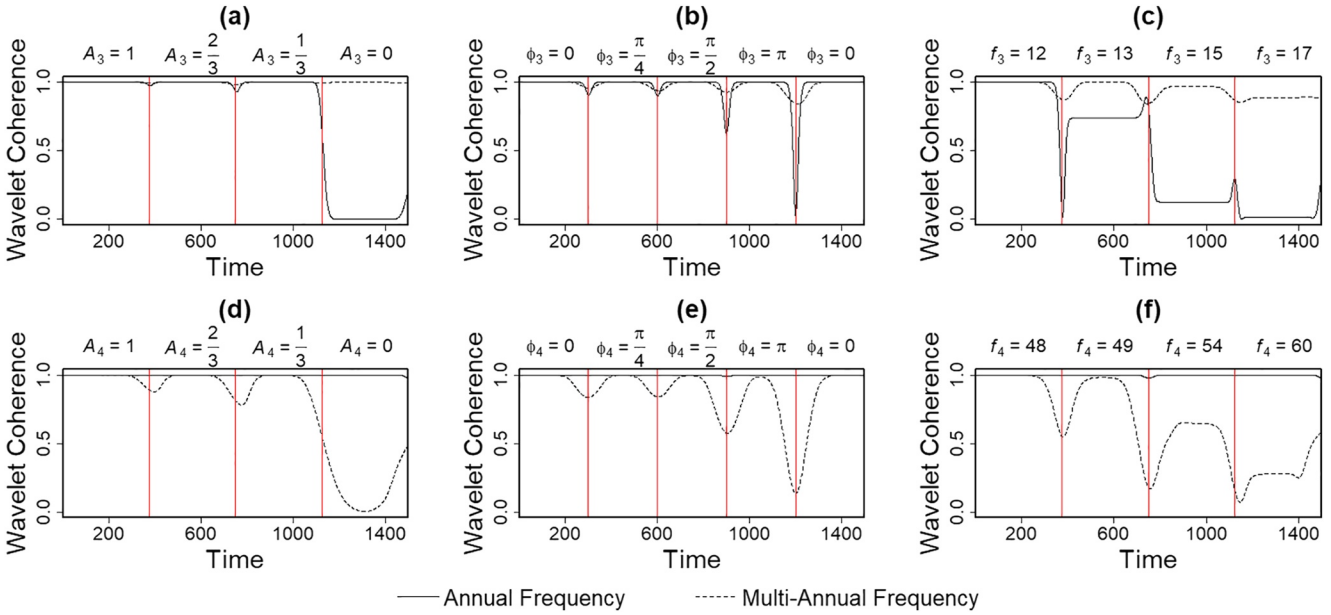

Figure 3. Wavelet coherence simulations between two synthetic sinusoidal time series y_1 and y_2. The simulated time series y_1 and y_2 were initially set to be identical to each other, and one wave component of y_2 was forced to change over time for each simulation while the other components remained fixed. The time-varying wavelet coherence between y_1 and y_2 was estimated when the amplitude component of the annual signal of y_2 (A_3) changes over time (a), when the phase lag component of the annual signal of y_2 (φ_3) changes over time (b), and when the phase lag component of the annual signal of y_2 (f_3) changes over time (c). Similarly, the simulation measures wavelet coherence between y_1 and y_2 when the amplitude component of the multi-annual signal of y_2 (A_4) changes over time (d), when the phase lag component of the multi-annual signal of y_2 (φ_4) changes over time (e), and when the phase lag component of the multi-annual signal of y_2 (f_4) changes over time (f).

completely removed, changes in amplitude had a minor impact on wavelet coherence — if entirely removed, wavelet coherence exhibited a significant downward shift.

Wavelet coherence finds locally phase-locked behaviors (Grinsted et al., 2004), and therefore, changes in the phase difference between two signals have a minimal impact on the fluctuation of the wavelet coherence at any frequency level (Figures 3b and 3e). However, it is shown from the simulation that the wavelet coherence drastically decreases and recovers whenever one of the signals changes its phase by π. Instantaneous fluctuations in the wavelet coherence caused by this phase shift can be detected by comparing the phase differences between the signals before and after the expeditious fluctuation.

As expected, wavelet coherence showed the most sensitive response to changes in frequency (Figures 3c and 3f). Wavelet coherence began to shift as soon as the frequency of signals started to differ from each other. The larger the frequency change, exponentially more the wavelet coherence was lost. During these simulations, it was confirmed that the temporal resolution of wavelet coherence was lower in the multi-annual frequency band than in the annual frequency band. Wavelet coherence responded immediately to changes in the relationship between the signals in the annual frequency band, while it tended to lag in the multi-annual frequency band. This observation reflects the tradeoff between the temporal and frequency resolutions of the wavelet. To summarize the simulations, fluctuations in wavelet coherence could be affected by any wave component, but permanent shifts were only induced by changes in frequency.

Figure A1 presents an example of the wavelet coherence analysis between the naturalized and controlled flows downstream of Glen Canyon Dam. Streamflow amplitude decreased remarkably after the construction of Glen Canyon Dam in 1963 (Figures A1d and A1e), and the annual frequency of streamflow diminished (Figures A1a and A1b). However, considering the findings from our experiments, the significant decline in wavelet coherence between naturalized and controlled flows in both the annual and multi-annual frequency bands (Figures A1c and A1f) was presumed to be dominantly caused by the distortion in the frequency component of streamflow. The inferences from this experiment were then used to better explain wavelet coherence results for the CRB.

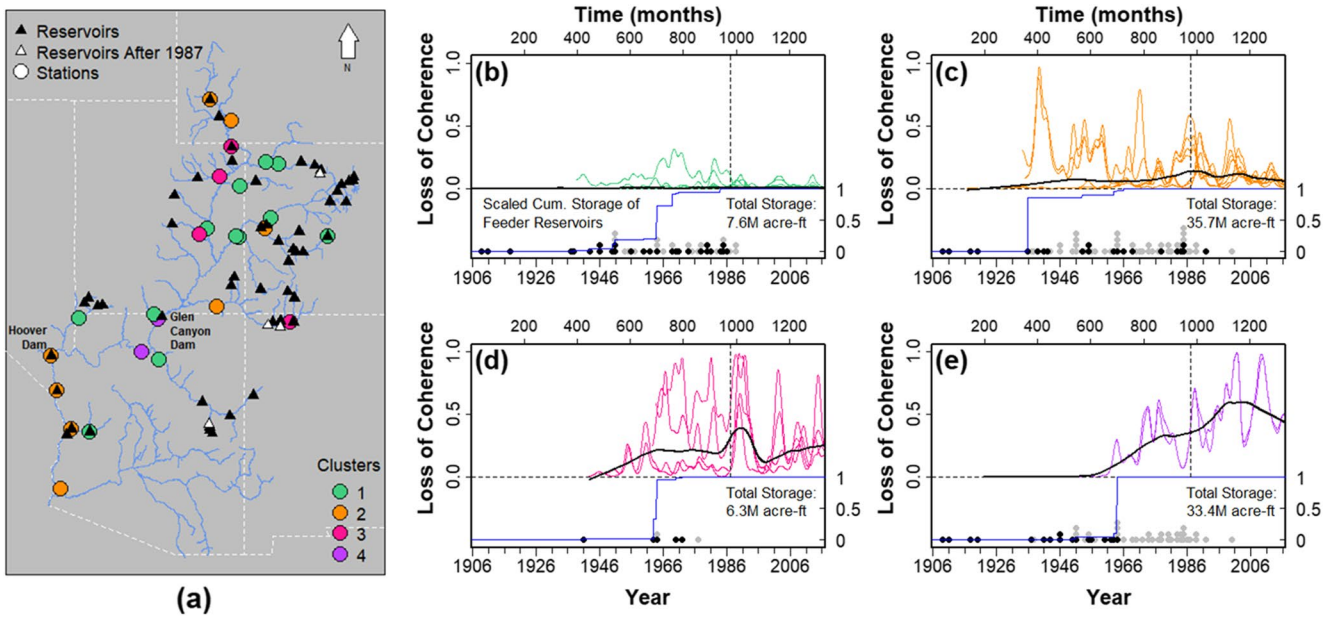

Figure 4. Cluster profiles based on wavelet coherence loss of streamflow regarding annual frequency (10–14 months). The spatial distribution of the clusters (a) and time series of wavelet coherence loss at each cluster (b–e) is shown. Each cluster is assigned with different colors, as shown in the map, and its time series of wavelet coherence loss is displayed following the same color scheme. Each set of time-varying wavelet coherence loss is locally fitted (LOWESS) for each cluster and is shown with a solid black line. The vertical dashed line indicates year 1987. In the lower part of each subplot, upstream reservoirs' construction timing is depicted for each cluster, with black and gray points over time. Black points indicate construction of immediate upstream reservoirs, which directly fed the cluster at that time, whereas gray points represent the installation of upstream reservoirs with indirect impact. Change in immediate upstream reservoirs' total storage capacity is shown in a scaled measure for each cluster (solid blue line). The fitted line for cluster 1 is overlapped with the zero-base line.

4. Results

As a result of DTW-based hierarchical clustering, the 26 streamflow gaging stations were classified into four clusters for both the annual and multi-annual frequency bands. Figures 4 and 5 show the stations constituting each cluster and the behavior of wavelet coherence loss for each cluster in the annual and multi-annual frequency ranges, respectively. Panel (a) of Figures 4 and 5 show the spatial distribution of the 26 stations and the cluster they belong. Panels (b) to (e) show wavelet coherence loss time series for the stations representing the clusters. While the DTW-based hierarchical clustering was applied to 1987–2016 data, wavelet coherence loss for the entire time series is shown in these panels. Dam constructions are also illustrated in these figures, with the evolution of each cluster's cumulative reservoir capacity. The time-varying wavelet coherence loss between naturalized and controlled streamflow is qualitatively explained for each cluster and frequency band – their collective characteristics in relation to the climate and anthropogenic conditions. We assumed that naturalized flow represents climatic conditions. For each station, the mean annual naturalized flow was divided into three categories based on the terciles (33 percentile and 66 percentile), each representing a dry, neutral, and wet year, in ascending order.

4.1. Annual Frequency

Based on wavelet coherence loss at the annual frequency, the river network of CRB was clustered into four groups. The annual frequency component was relatively well preserved across the basin even in areas where streamflow was heavily regulated, such as the downstream of Hoover Dam, whereas some tributaries in the UCRB have been showing significant variability in the annual wavelet coherence loss. The section immediately downstream of Glen Canyon Dam has been systematically losing its annual frequency since the construction of Glen Canyon Dam in 1963.

The first cluster included eight stations from the UCRB and four stations from the tributaries in the LCRB (Figure 4a). The time series of wavelet coherence loss for these 12 stations show that streamflow lost

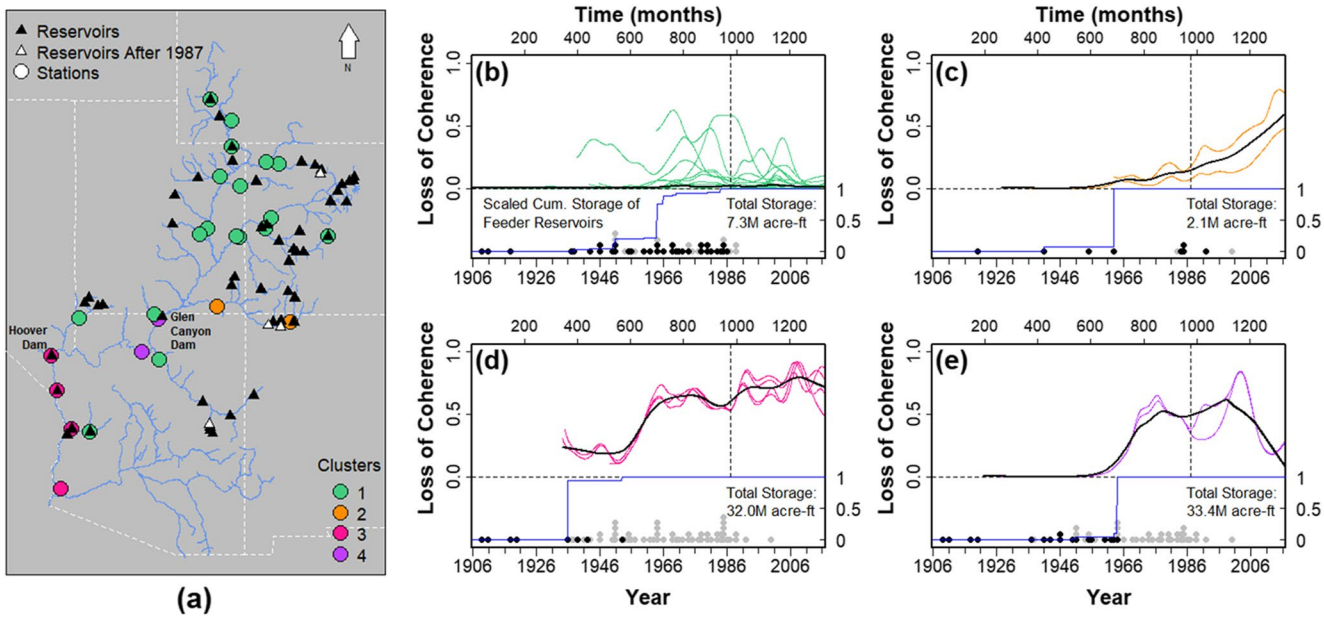

Figure 5. Cluster profiles based on the wavelet coherence loss of streamflow regarding multi-annual frequency (24–60 months). The spatial distribution of the clusters (a) and time series of the wavelet coherence loss at each cluster (b–e) is shown. Rest of the figure is similar to the description provided in Figure 4.

coherence with the naturalized flow by less than 33% (low coherence loss) in terms of annual frequency at these stations since 1987 (past 30 years) (Figure 4b). This suggests that anthropogenic influences such as management have had little to minimal impact on annual frequency of streamflow at these locations.

Cluster-2 consisted of eight stations, four of which are located along the Colorado River after Hoover Dam, and the rest along tributaries of the UCRB (Figure 4a). It is notable that the Colorado River below Hoover Dam shows similar behavior to the UCRB tributaries in terms of annual frequency. Average wavelet coherence loss was 11%, and an evident temporal variation was observed at these stations (Figure 4c). The probability of wavelet coherence loss exceeding 66% (high coherence loss) was negligible at these eight stations for years 1987–2016. Coherence loss was mostly less than 33% (low coherence loss) during those years, regardless of the annual climate conditions. As shown in Figure 4c, this cluster consisted of two groups of stations that exhibited different behaviors in the earlier years (1930–1980). During this period, the Colorado River downstream of Hoover Dam exhibited more temporal variability in wavelet coherence loss than the more recent 30-year period, while UCRB tributaries showed a constant behavior.

The third cluster contained four stations in the UCRB, mostly in tributaries regulated by dams (Green River, San Juan River, San Rafael River, Duchesne River) (Figure 4a). Average wavelet coherence loss of streamflow at these stations was 28%, and significant interannual variability was observed (Figure 4d). Wavelet coherence loss at two of these stations (San Rafael River, Duchesne River) tended to be relatively greater during dry years (e.g., 1988, 1989, 1990, 2002, 2003, 2004). In contrast, wavelet coherence was preserved during wet and dry years at the Green and San Juan Rivers. The probability of wavelet coherence loss being less than 33% (low coherence loss) was 72% on average across stations. When examining climatically wet and dry years, the probability remained high (58%–81%). The overall probability of losing wavelet coherence by 33%–66% (medium coherence loss) was 19%. Depending on climatic conditions, this probability became 7% under wet conditions, 25% under neutral conditions, and 25% under dry conditions (on average). The probability of wavelet coherence loss being greater than 66% (high coherence loss) at these four stations was 10% on average. Under drier conditions, wavelet coherence loss exhibited a higher probability of exceedance (11%–38%) except at one station (San Juan River), where exceedance never occurred over the given 30-year period.

Wavelet coherence loss estimates at these stations showed a synchronized pattern of fluctuation over time since the 1980s. To explain this better, we explored wavelet coherence in (annual frequency) between the

naturalized flow series of these four stations with one another (i.e., coherence between the natural flows of San Rafael River and Duchesne rivers, San Rafael River and Green River, San Rafael River and San Juan River, Duchesne River and Green River, Duchesne River and San Juan River, and Green River and San Juan River) (Figures A2–A6). We confirmed a high level of synchronicity regardless of their distant location. This shows that these four stations have a high degree of co-variability in their naturalized flows, indicating that regional climatic fluctuations at these locations are very similar. The fact that wavelet coherence loss estimates at these stations between natural and controlled flows show a synchronized pattern of fluctuation over time (since the 1980s) also indicates they have a high degree of co-variability in controlled flows, indicating a synchronized alteration – similar anthropogenic forcing. In other words, streamflow at these four stations may have been under similar controls in terms of annual frequency since the 1980s. As shown in Figure 4d, significant shifts in wavelet coherence loss can be observed since 1987. These shifts can occur when the annual frequency is particularly disrupted in either the naturalized or controlled streamflow. According to the wavelet power spectra, controlled flows had a weak annual frequency signal during the shifts, whereas naturalized flows showed statistically significant annual frequency signals for most of the time at these four stations (Figure A2). The significant shift of wavelet coherence loss that occurred at Cluster-3 in the 1980s is reflected in the *Final Biological Opinion on the Operation of Flaming Gorge* issued by the U.S. Fish and Wildlife Service in 1992. The opinion stated that Flaming Gorge Dam's operation would endanger the aquatic biota and riparian ecology of the Green River (U.S. Fish and Wildlife Service, 1992). During this time, additional constructions for water storage facilities were planned, and hydrologic assessments suggested that ecological impacts could be partially counterbalanced by flexibly changing the operation of Navajo Dam (U.S. Fish and Wildlife Service, 1991). In 1993, the U.S. Bureau of Reclamation started to alter the operation of these dams to meet flow recommendations outlined in the 1992 Final Biological Opinion. This operational change coincides with the recovery of the wavelet coherence loss of the cluster.

Lastly, the fourth cluster consisted of two sequential stations in the Colorado River mainstem below Glen Canyon Dam (Figure 4a). Their overall average wavelet coherence loss was 54%, and a systematic loss in wavelet coherence was observed with a quasi-cyclical variability (Figure 4e). Trends in wavelet coherence loss at these two stations were tested using the Mann-Kendall test (Kendall, 1948; Mann, 1945), both showing a statistically significant upward trend (*Mann-Kendall tau = 0.68, 0.71; p-value* < 0.01). The beginning of this trend coincided with the completion of Glen Canyon Dam in 1963. The wavelet power spectrum of naturalized flow at these stations indicates that the annual frequency signal is statistically significant across the study period. In contrast, the annual frequency signal in controlled flow at these stations is mostly diminished (Figure A3). Therefore, the systematic increase in wavelet coherence loss observed in Cluster-4 is assumed to be due to anthropogenic factors rather than to climate. At this point it would be premature to conclude that Glen Canyon Dam's operations are the dominant cause for the distortion. It is possible for streamflow to exhibit high levels of frequency distortion even while its immediate upstream reservoirs pass on their upstream hydrograph. That is, wavelet coherence loss of streamflow could propagate from upstream as affected by other dams, while the dams located immediately upstream operate in a way that do not alter streamflow frequency. Details of this aspect will be discussed in Section 4.3. Meanwhile, the probability of observing coherence loss greater than 33% (medium or high coherence loss) at these two stations was 89% and 79% respectively, and probabilities of coherence loss exceeding 66% (high loss) were both 30%. Regardless of climate, the average probability of exceedance remained significant (Wet: 29%, Neutral: 35%, Dry: 22%). Specifically, wavelet coherence loss (WCL) at the station immediately below the Glen Canyon Dam had a probability $P(WCL > 0.66) = 0.29$, while $P(WCL > 0.66|Wet) = 0.29$ and $P(WCL > 0.66|Dry) = 0.22$. At the other station, $P(WCL > 0.66) = 0.31$, and $P(WCL > 0.66|Wet) = 0.33$, $P(WCL > 0.66|Dry) = 0.23$. Wavelet coherence loss of streamflow at these two stations showed a similar modality despite tributaries joining between them.

4.2. Multi-Annual Frequency

The analysis of wavelet coherence loss for multi-annual frequency classified the river network into four different clusters: all rivers of UCRB (except San Juan River) and tributaries in LCRB (Cluster-1), the San Juan River (Cluster-2), a segment of the Colorado River below Hoover Dam (Cluster-3), and the section immediately downstream of Glen Canyon Dam (Cluster-4). While wavelet coherence loss of multi-annual frequency remained at a relatively low level in most UCRB rivers, significant losses were observed in other

regions. A systematic increase in wavelet coherence loss has been observed since completion of Navajo Dam in 1962. The section immediately downstream of Glen Canyon and Hoover Dams has shown a high level of alteration in the multi-frequency component, but the downstream of Glen Canyon Dam has been recently recovering its wavelet coherence loss.

The first cluster comprised 14 stations from the UCRB and four stations in the LCRB tributaries (Figure 5a), for a total of 18 stations. As shown in Figure 5b, estimated wavelet coherence loss was relatively low at these stations, with an average of 4% for the multi-annual frequency band. Wavelet coherence loss never exceeded 66% at these stations, regardless of climate conditions (dry or wet years). A few stations showed moderate levels of wavelet coherence loss ($33\% < WCL < 66\%$) during a few months, but most of the losses were lower than 33% (low coherence loss) over the study period. This cluster contained all 12 stations of Cluster-1 from the annual frequency analysis. Moreover, three stations classified as Cluster-2 from the annual frequency analysis were also included in this cluster. Cluster-1 and Cluster-2 from the annual frequency analysis represented stations with little to no coherence loss in the annual frequency. That is, those 15 stations retained a low level of modification at both the annual and multi-annual frequency scales.

The second cluster consisted of two stations in the San Juan River (Figure 5a). As shown in Figure 5c, a systematic increase in the multi-annual wavelet coherence loss was observed at these two stations (Mann-Kendall tau = 0.84, 0.81; p-value < 0.01). This trend began to develop with the completion of Navajo Dam, the largest dam on the San Juan River. This systematic increase may be attributable to the drastic reduction of the multi-annual frequency in the controlled flow, which can be observed from its wavelet power spectrum (Figure A4). The increasing trend in multi-annual wavelet coherence loss in the San Juan River is assumed to be mainly driven by dam operations or other anthropogenic factors. To determine whether Navajo Dam had a significant impact on coherence loss in the San Juan River, the dam's local regulation was assessed by investigating wavelet coherence upstream vs. downstream of the dam (see Section 4.3). One station of this cluster is located downstream of the other and was classified as Cluster-2 from the annual frequency analysis, showing little to no coherence loss in the annual frequency range. The other station is immediately downstream of the Navajo Dam and belonged to Cluster-3 of the annual frequency analysis, exhibiting significant interannual variability in the annual wavelet coherence loss. Both the annual and multi-annual signals in the San Juan River were disrupted in the upstream, and the annual frequency partially recovered as the streamflow proceeds along the river. However, the disruption of the multi-annual signal mostly propagated downstream.

The four stations along the Colorado River mainstem below Hoover Dam were grouped as Cluster-3 (Figure 5a). The multi-annual wavelet coherence loss at these four stations was high, 73% on average since 1987, with some temporal variability (Figure 5d). Interestingly, these four stations had been categorized as Cluster-2 in the annual frequency analysis, with little to no coherence loss in the annual frequency range. In other words, streamflow at these four stations had lost its coherence in terms of multi-annual frequency, while the annual frequency feature was preserved (during the 30-year study period). A shift in wavelet coherence loss was observed at these four stations in the 1950s after the construction of Davis Dam. The multi-annual frequency wavelet power spectrum of controlled flow exhibited a deflation in both variability and scale-averaged power since dam completion. In contrast, a consistent quasi-oscillatory signal of the multi-annual frequency component was observed in the wavelet power spectrum of naturalized flow across the 30-year period (Figure A5). These observations led us to assume that an operational change to the local dams after construction of Davis Dam partially diminished the local streamflow's coherence with its naturalized flow at the multi-annual scale. The Mexican Water Treaty of 1944 ensured the construction of Davis Dam to regulate and deliver annual flow to Mexico (U.S. Bureau of Reclamation, 1946), which, in turn, likely contributed to the recovery of annual frequency in streamflow downstream of Davis Dam.

Cluster-4 comprised two sequential stations in the Colorado River below Glen Canyon Dam (Figure 5a). A recovery in multi-annual wavelet coherence was observed at these stations during the past 30 years. Over the extended time series shown in Figure 5e, wavelet coherence loss increased dramatically as Glen Canyon Dam's construction started in 1956, and it has recently been decreasing. The ascending shift in wavelet coherence loss may result from the multi-annual frequency signal's subsidence in the controlled streamflow, which can be observed in its wavelet power spectrum (Figure A6). The recent decrease in wavelet coherence loss reflects a recovery of the local correlation in multi-annual frequency signal between naturalized and

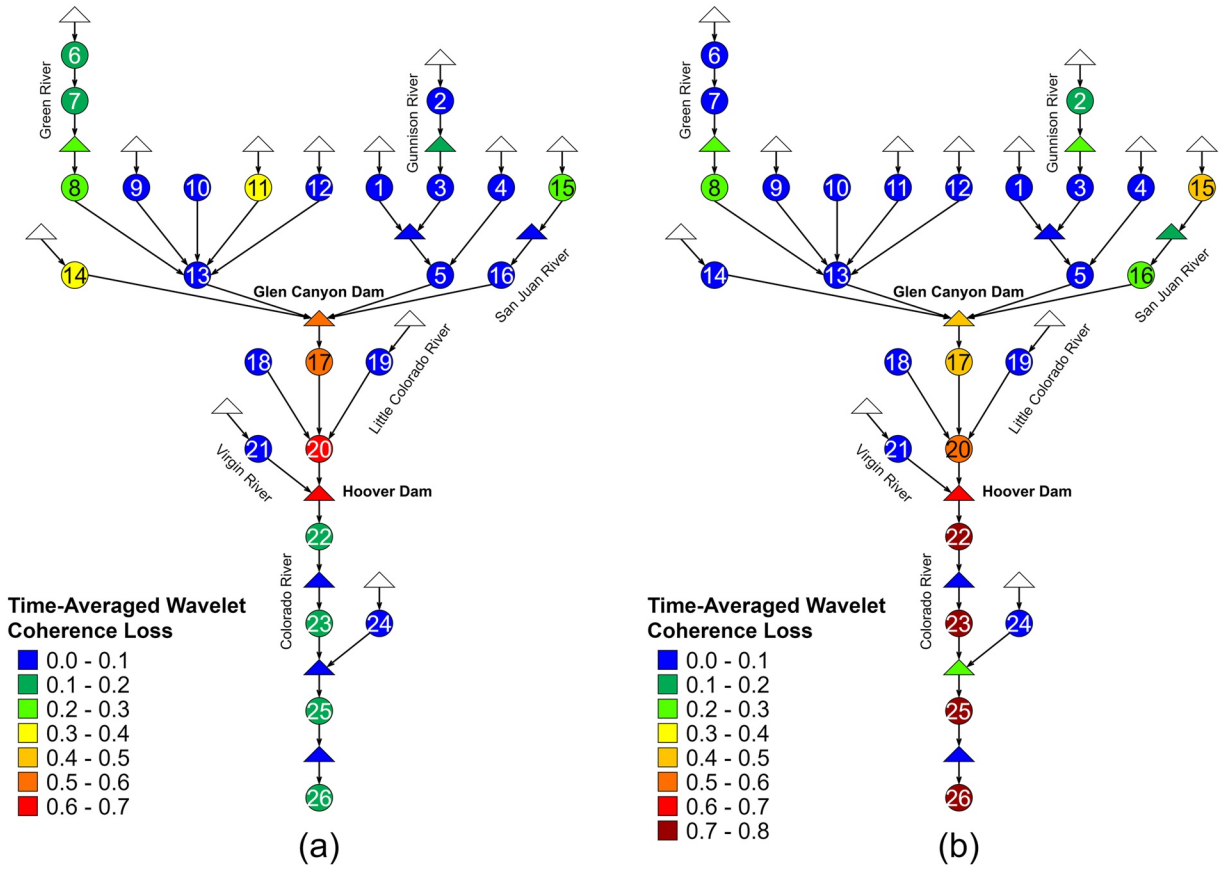

Figure 6. Simplified diagram of the riverine network with local and cumulative streamflow alteration measured for both the annual (a) and multi-annual frequency bands (b). Dam-induced local regulation is represented with triangles, and cumulative alteration is denoted with circles.

controlled flows. The mean probability of wavelet coherence loss exceeding 66% (high coherence loss) at these two stations is 0.36.

4.3. Local Impacts of Dams on Frequency Alteration

In previous sections we focused on stations where streamflow showed significant distortion in frequency and examined whether it was mainly due to anthropogenic factors or changes in the regional climate. Even if frequency loss at a given station is presumed to be driven by anthropogenic factors, the distortion does not need to take place immediately upstream of the station – it could have been increasing cumulatively over the entire network. To identify reservoirs or group of reservoirs with significant contributions to such streamflow alteration, we computed the time-averaged wavelet coherence loss between the controlled flow series upstream and downstream of each dam cluster, for both the annual and multi-annual frequency bands. Local regulation was ascribed to dams that regulate flow between upstream-downstream pair(s). In addition, the time-averaged wavelet coherence loss between the naturalized and controlled streamflow series was computed for each station and frequency band. We assumed this metric captures cumulative alteration across the river network.

Local regulation and cumulative discordance for both the annual and multi-annual frequency bands are shown in Figure 6 with a simplified riverine network diagram. The figure presents the time-averaged wavelet coherence loss between naturalized and controlled flow in circles across the basin, and they indicate the cumulative alterations in frequency. Meanwhile, the time-averaged wavelet coherence loss between the upstream and downstream controlled flow series of each dam or dam cluster is shown in triangles – they represent local alteration in frequency due to the corresponding dam or dam cluster. We found that the annual frequency of streamflow was less cumulatively altered at most of the stations in the UCRB. Alteration on

annual frequency generally became more perceptible as the river proceeded, especially after Glen Canyon Dam, but it eventually recovered (as it passed Hoover Dam). The annual frequency signal of streamflow at station 15 (San Juan River near Archuleta, NM) in the San Juan River was moderately regulated, and the downstream group of dams showed a low level of local regulation on the annual frequency signal of streamflow (0.09). Consequently, streamflow recovered its distorted annual frequency signal by the time it reached station 16 (San Juan River near Bluff, UT). This recovery may be induced by confluences of tributaries with a robust annual frequency signal. Glen Canyon Dam showed a significant impact on the local streamflow's annual periodicity (0.58), and it propagated to station 20 (Colorado River near Grand Canyon, AZ). Hoover Dam seemed to heavily regulate the annual frequency of the local streamflow (0.56), but in a way that got closer to the "naturalized" annual frequency. This could be partially due to the Mexican Water Treaty of 1944, where the U.S. agreed to commit 1,850 million m^3 of the Colorado River's annual flow to Mexico (U.S. Bureau of Reclamation, 1946) at scheduled monthly minimum agreements. Dams on the mainstem downstream of Hoover Dam had minimal impact on the annual frequency. Therefore, streamflow regime characteristics at these four stations in Cluster-2 arise from local regulation at Hoover Dam and the operation of subsequent dams "inheriting" upstream hydrographs.

The multi-annual frequency feature of streamflow was less altered in the UCRB, except in the San Juan River. The multi-annual frequency component of the Colorado River below Glen Canyon Dam showed a high degree of alteration and became even higher as it passed through Hoover Dam. For the multi-annual frequency scale, a significant degree of cumulative alteration was observed at station 15 (San Juan River near Archuleta, NM), and it propagated down the San Juan River. This cumulative distortion of the San Juan River's multi-annual frequency was partially recovered reaching station 16 (San Juan River near Bluff, UT), but not enough to resemble its natural state. For both the annual and multi-annual frequency bands, the cluster of reservoirs that directly fed station 16 (San Juan River near Bluff, UT) showed negligible local regulation (0.17). Considering there are no major dams in the San Juan River other than those feeding station 15 (San Juan River near Archuleta, NM) and 16 (San Juan River near Bluff, UT), the mutual behavior of streamflow at these stations for the multi-annual frequency, shown in Cluster-2 of the multi-annual frequency analysis, is assumed to be driven by management of the Navajo Dam. Glen Canyon Dam significantly regulated the multi-annual frequency component of local streamflow (0.41). Since there are no major dams in the river segment that significantly affects the multi-annual frequency signal of the streamflow between station 17 (Colorado River at Lees Ferry, AZ) and 20 (Colorado River near Grand Canyon, AZ), the mutual pattern of wavelet coherence loss of multi-annual frequency (shown in Cluster-4) is likely due to the local regulation of Glen Canyon Dam. Hoover Dam also had significant control over the multi-annual frequency signal of local streamflow (0.64), and downstream of the dam showed a consistent pattern in wavelet coherence loss. There are three major dams downstream of Hoover Dam (Davis, Parker, Headgate Rock), which have negligible local impacts on the cumulative distortion of the multi-annual frequency band (0.05, 0.25, 0.06). This observation suggests that local regulation of Hoover Dam drives the observed multi-annual frequency coherence loss in Cluster-3.

5. Discussion

This study focused on quantifying streamflow alteration particularly the contribution from local dams over the CRB. However, joint operations of dams within the basin collectively control flow and propagate alteration from the headwaters to the lower sections of the CRB. Detailed information of operation rules of reservoirs is difficult to extract particularly for multi-purpose reservoirs with complex treaties. Hence, joint operations were indirectly explored by focusing on compacts, decrees, contracts, and regulatory guidelines for the CRB. The Colorado River Compact of 1922 divided the CRB into upper and lower halves and required the upper basin to maintain the annual flow at Lee Ferry (below Glen Canyon Dam) at least 9,250 million m^3 (U.S. Bureau of Reclamation, 1922). This compact may have contributed to the distinct difference between flow alteration patterns at UCRB and LCRB as shown in Figure 6. The natural annual frequency band was mostly preserved in the upper basin. In turn, the restoration of the annual frequency by Hoover Dam and preservation of the restored annual frequency by subsequent dams (Figure 6a) could be related to the Mexican Water Treaty of 1944, which defines biannual allotment of water delivery from the Colorado River to Mexico at the monthly scale (U.S. Bureau of Reclamation, 1946). This complex water policy and

management framework hinders precise attribution of streamflow alteration, and future studies could build on our efforts by examining joint operations via release data of each reservoir.

This study assessed the cumulative and local impacts of dams on flow frequencies to better understand how altered flow frequencies propagate through river networks – a critical need in highly regulated basins. Our approach focused on explaining spatiotemporal changes in frequency components of streamflow and could help prioritize sites for restoration or environmental flow operations (Palmer & Ruhi, 2019). Studies have been conducted to establish frameworks for environmental management of reservoirs (Richter & Thomas, 2007; Wang et al., 2015; Yang & Cai, 2011), as environmental flow operations and/or preservation of free-flowing tributaries may help restore specific dimensions of flow variability (e.g., at daily and seasonal scales). Preserving natural patterns of flow variability, and not just annual flow magnitudes, has shown to contribute to native biodiversity conservation, while the contrary (flow "stabilization") has shown to favor biological invasions across the U.S. rivers (e.g., Comte et al., 2021). Because the frequency component of streamflow is often strongly coupled with key life histories of riparian and riverine organisms, such as seasonal reproduction and dispersal events (Bain et al., 1988; Lytle & Poff, 2004; Richter et al., 1996), alterations in the frequency domain are often ecologically consequential. Thus, the proposed approach could contribute to identifying river reaches and times when alteration of a specific frequency could be particularly damaging from an ecological standpoint.

Many other methods exist to quantify human-induced hydrologic changes, such as the *Indicators of Hydrologic Alteration* (*IHA*; Chalise et al., 2021; Poff et al., 2010; Richter et al., 1996). The IHA method is based on 32 hydrologic metrics that describe five different facets of the flow regime, including magnitude, duration, timing, and frequency of high and low flow pulses. However, IHA and similar methods often require splitting the time series, so that part of it is used as a reference (e.g., pre-dam conditions) against which to compare the second part. In contrast, our approach allows localizing changes in amplitudes of each targeted frequency in a continuous way, without having to pre-specify a "reference" and an "impact" period. Additionally, wavelet-based methods allow targeting multiple frequencies at the same time – from multi-annual to seasonal and even diel (if sub-daily data are available), as opposed to the annual focus of more traditional approaches. Since our proposed approach is based on the naturalized flow data, however, its application is limited by the availability and accuracy of the naturalized flows. Uncertainties in the estimation of naturalized flows could propagate as errors in the wavelet coherence analysis between controlled and naturalized flows. Nevertheless, for assessing the impacts of hydrologic alteration on river ecosystems, we contend our approach has two key advantages: First, because climate non-stationarity may mean that 'static' hydrologic references from the past are no longer relevant to contemporary alteration (Poff, 2018). Second, because focusing on particular frequencies while overlooking others could lead to fundamentally underestimating true alteration, particularly if low frequencies (e.g., annual flow cycles) are close to natural levels but 'unexpected' frequencies are introduced at various time scales (e.g., daily (hydropower), weekly (irrigation) or decadal (water supply)) due to the multi-purpose nature of reservoir operations (Kennedy et al., 2016; Ruhi et al., 2018), hence highlighting the importance of resolving multiple scales (high and low frequency periodicities as related to the application at hand) in the time series.

6. Summary and Conclusions

This study estimated time-varying alteration in streamflow frequency in the CRB via wavelet coherence analysis between the naturalized and controlled streamflow series. Wavelet coherence loss between the naturalized and controlled flows represents the cumulative degree of alteration of the frequencies in streamflow propagated from the headwaters. Stations where streamflow showed similar patterns in wavelet coherence loss were grouped together, and four clusters were identified for each annual and multi-annual frequency band. At most of the stations in UCRB, the frequency component of the streamflow was relatively well preserved. Interestingly, the Colorado River after Hoover Dam showed a low degree of alteration in the annual frequency despite significant alteration induced by Glen Canyon Dam. In terms of multi-annual frequency, we observed significant levels of alteration downstream of Glen Canyon Dam. However, we observed a tendency to recover alteration of the annual frequency signal downstream of Hoover Dam. Meanwhile, the San Juan River has been showing a systematic increase in wavelet coherence loss for the multi-annual frequency since the completion of Navajo Dam in 1962.

The Colorado River in the Lower Colorado Basin could be divided into two river segments regarding the wavelet coherence loss – (a) from Glen Canyon Dam to Hoover Dam and (b) from Hoover Dam to the basin outlet. Wavelet coherence loss between Hoover and Glen Canyon Dam showed a homogeneous fluctuation across the segment, and the majority of this pattern was presumed to be caused by the local impact of Glen Canyon Dam. The pattern of wavelet coherence loss in the mainstem downstream of Hoover Dam showed uniformity in the annual frequency across the segment – we conclude that is "inherited" alteration from the Hoover Dam. Further, it also showed a similar pattern in the multi-annual frequency below Hoover Dam – we conclude that is "inherited" alteration from Glen Canyon Dam, further exacerbated by Hoover operations.

While we used CRB as a case study, our method allowed the quantification of time-varying alteration in the frequency domain, and the partitioning of anthropogenic from climate factors. Our approach is transferable to other highly regulated basins and could help better understand the propagation of dam-induced flow alteration, a critical need in the light of reoperation of existing infrastructure. Correspondingly, we emphasize the need of estimation of naturalized flows for large, regulated basins based on past releases, storages, and consumptive use. Because we had a naturalized flows dataset for a long period (Prairie & Callejo, 2005), we were able to analyze flow alteration at a multi-annual frequency band, which is influenced predominantly by water management. Simulating naturalized flow has been a challenge because of the limited information of human withdrawal and water management in addition to the absence of observed data for validation (Terrier et al., 2021). As a result, the naturalized flow data is currently available only for a small number of catchments in the United States. We contend that government and private agencies responsible for reservoir operations should coordinate and continue to make naturalized flows data available to support analyses such as ours. Future research evaluating streamflow frequency alteration could be improved by taking small dams and weirs into account – owing to their numbers, they often have substantial cumulative impacts (Couto & Olden, 2018). In addition, one may consider investigating streamflow alteration at finer temporal and frequency scales – with awareness of the tradeoff between time and frequency resolutions.

Appendix A

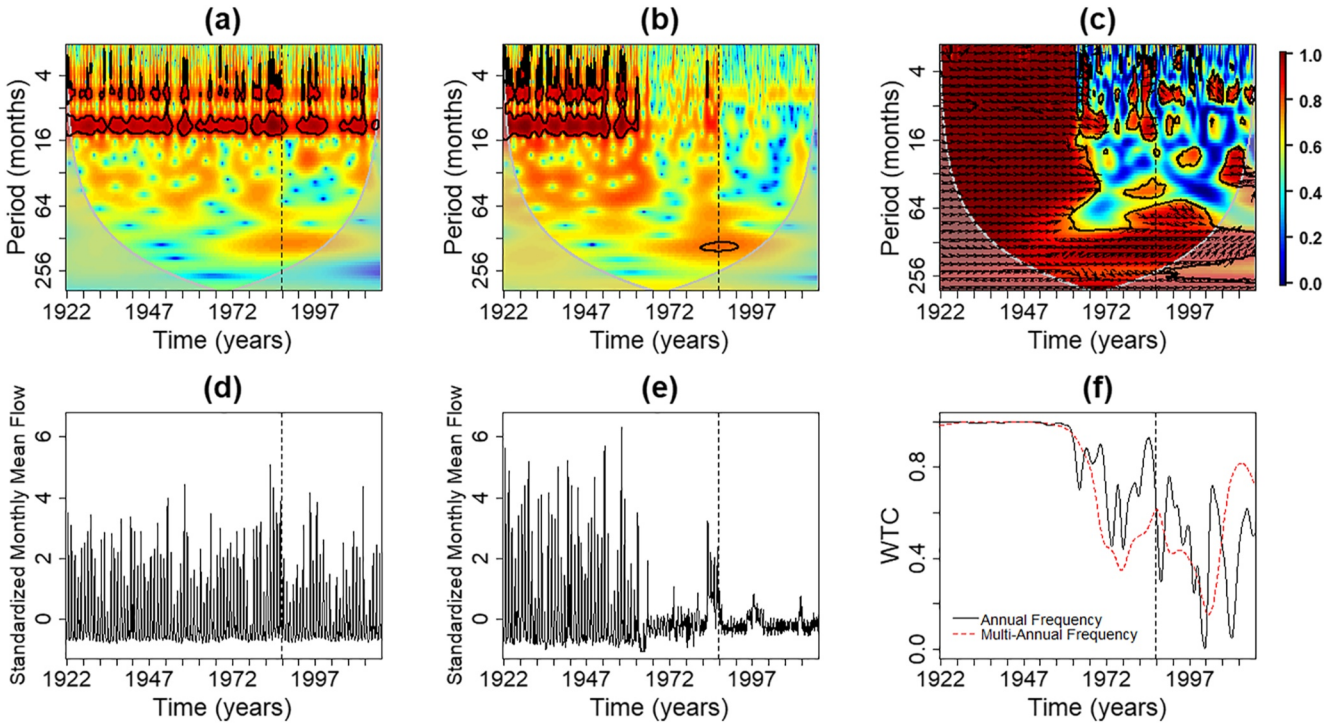

Figure A1. Wavelet coherence analysis between naturalized flow and controlled flow at the downstream of Glen Canyon Reservoir. Each subplot represents the wavelet power spectrum of the naturalized flow (a), wavelet power spectrum of the controlled flow (b), wavelet coherence spectrum between naturalized and controlled flow series (c), standardized monthly mean flow of the naturalized flow (d), standardized monthly mean flow of the controlled flow (e), and the scale-averaged wavelet coherence between naturalized and controlled flow series for annual and multi-annual frequency bands (f). The dashed line at 1987 indicates the beginning of the period of analysis for our study.

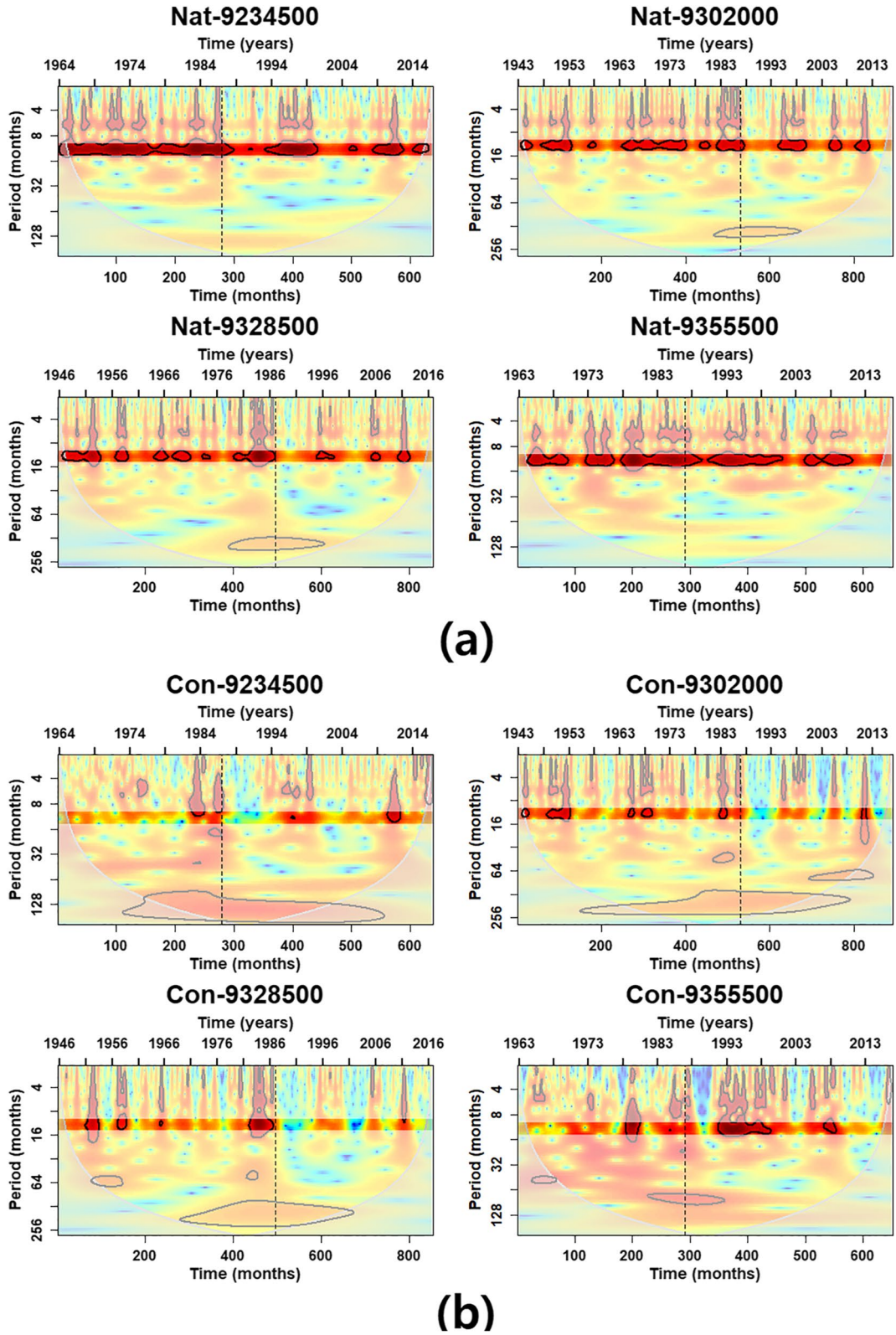

Figure A2. Wavelet power spectrum of the naturalized streamflow (a) and the controlled streamflow (b) at stations of Cluster-3 from the annual frequency analysis. Black contours in the spectra represent the 95% confidence level compared to red noise. The solid white line is the cone of influence, where zero padding has affected the variance. Red colors indicate higher local powers, whereas lower local powers are displayed in blue colors. The vertical dashed line indicates the year of 1987.

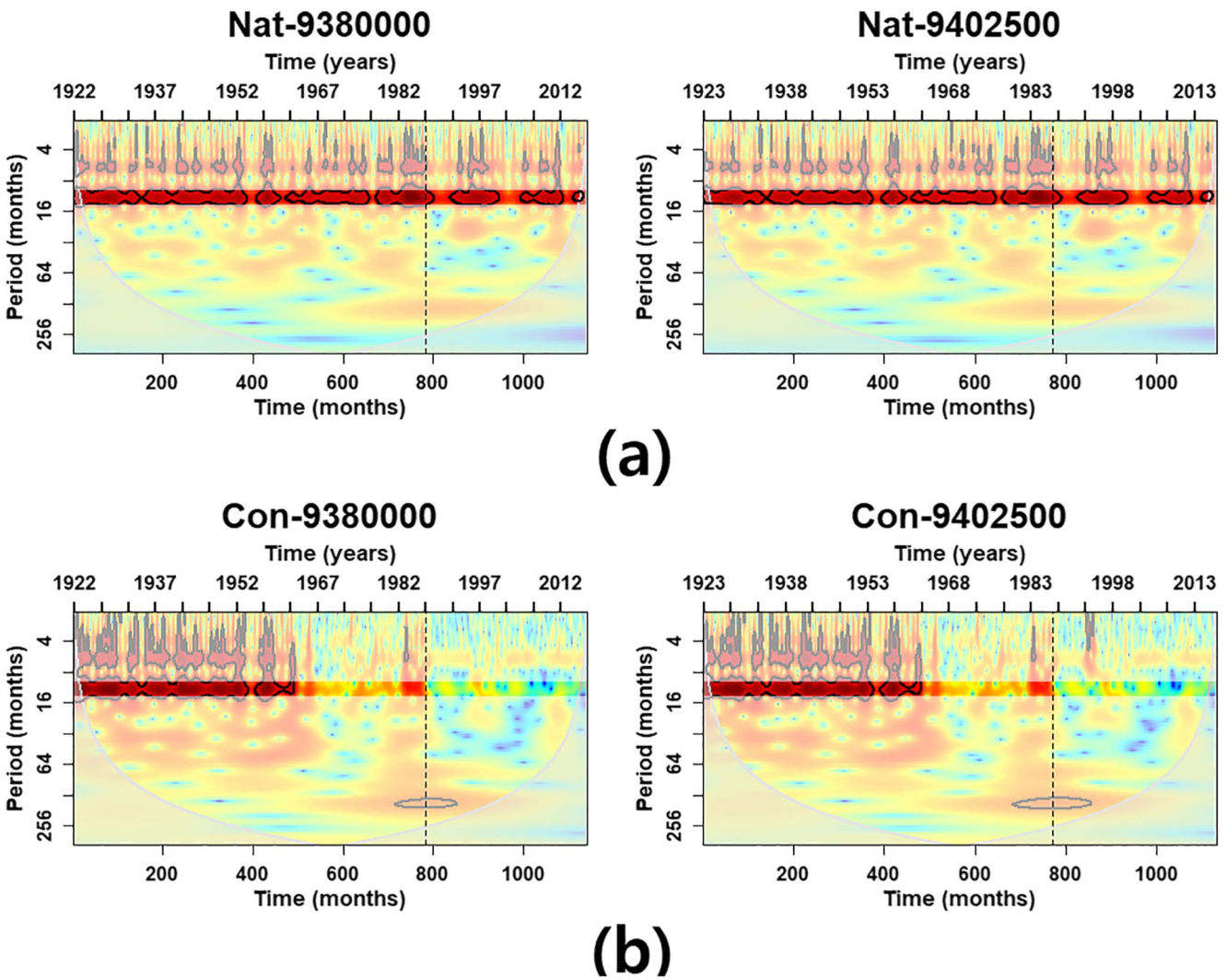

Figure A3. Wavelet power spectrum of the naturalized streamflow (a) and the controlled streamflow (b) at stations of Cluster-4 from the annual frequency analysis.

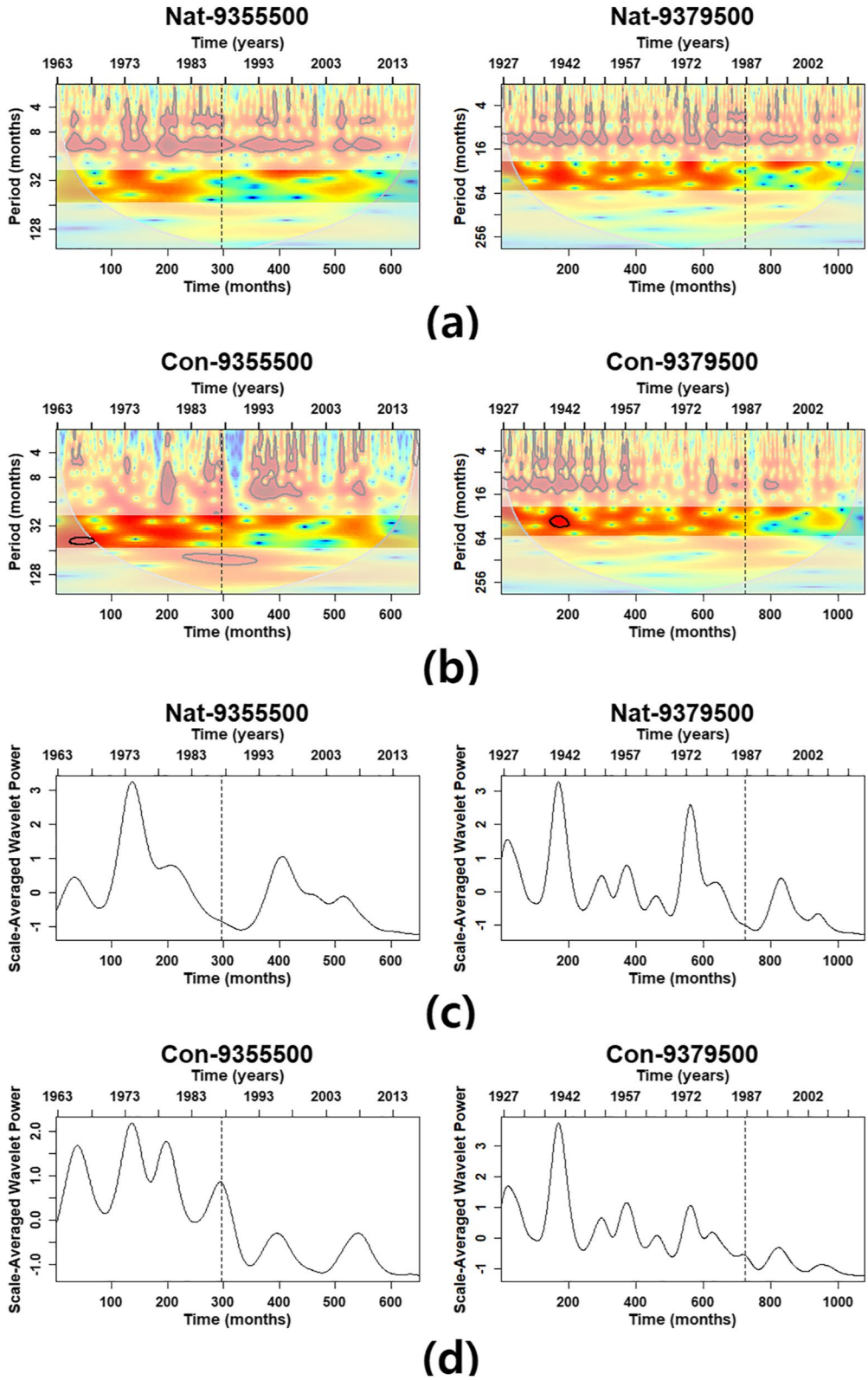

Figure A4. Wavelet power spectrum of the naturalized streamflow (a) and the controlled streamflow (b) at stations of Cluster-2 from the multi-annual frequency analysis. The scale-averaged wavelet power is also presented for both naturalized flow (c) and controlled flow (d) at these stations.

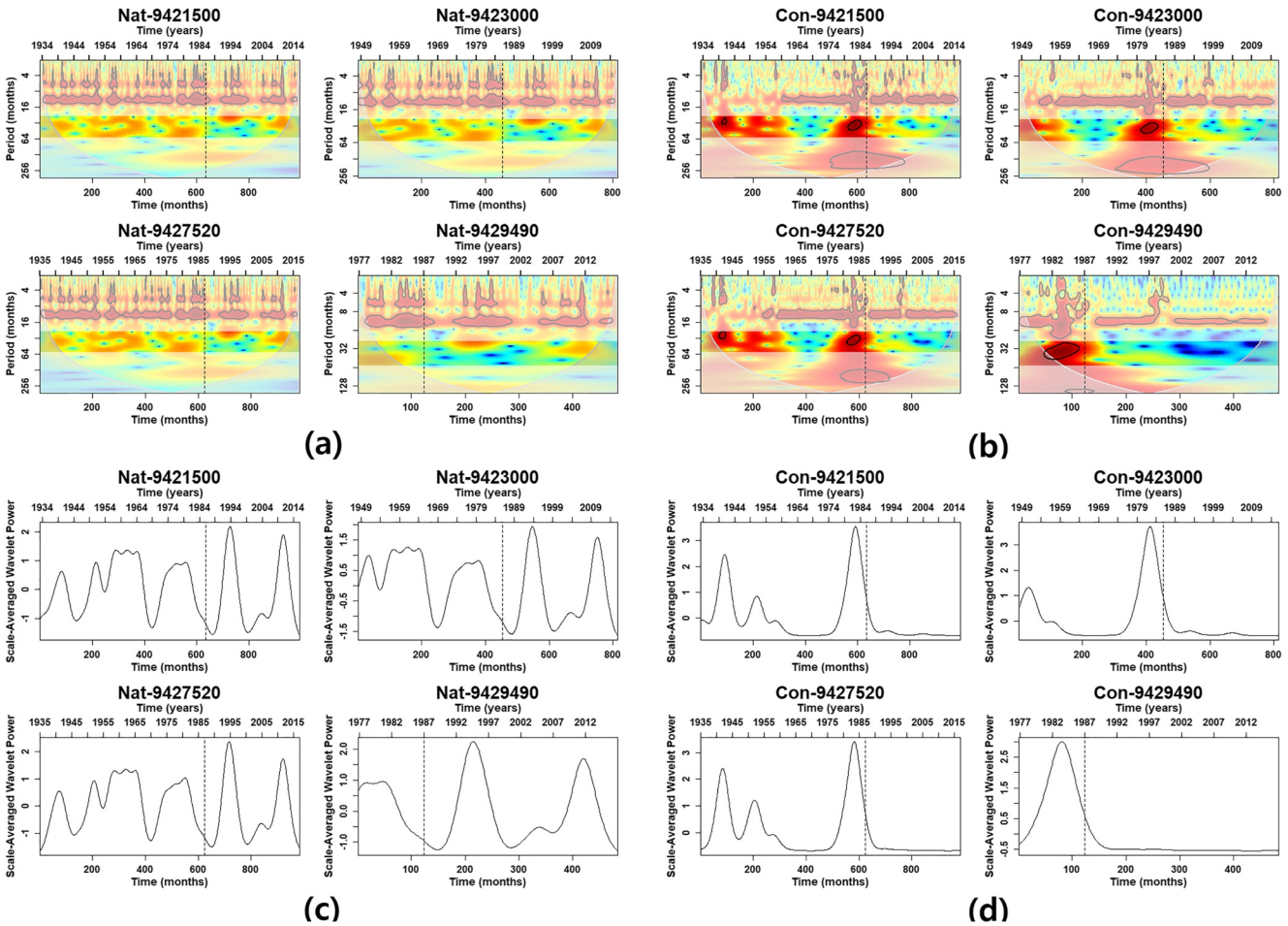

Figure A5. Wavelet power spectrum of the naturalized streamflow (a) and the controlled streamflow (b) at stations of Cluster-3 from the multi-annual frequency analysis. The scale-averaged wavelet power is also presented for both naturalized flow (c) and controlled flow (d) at these stations.

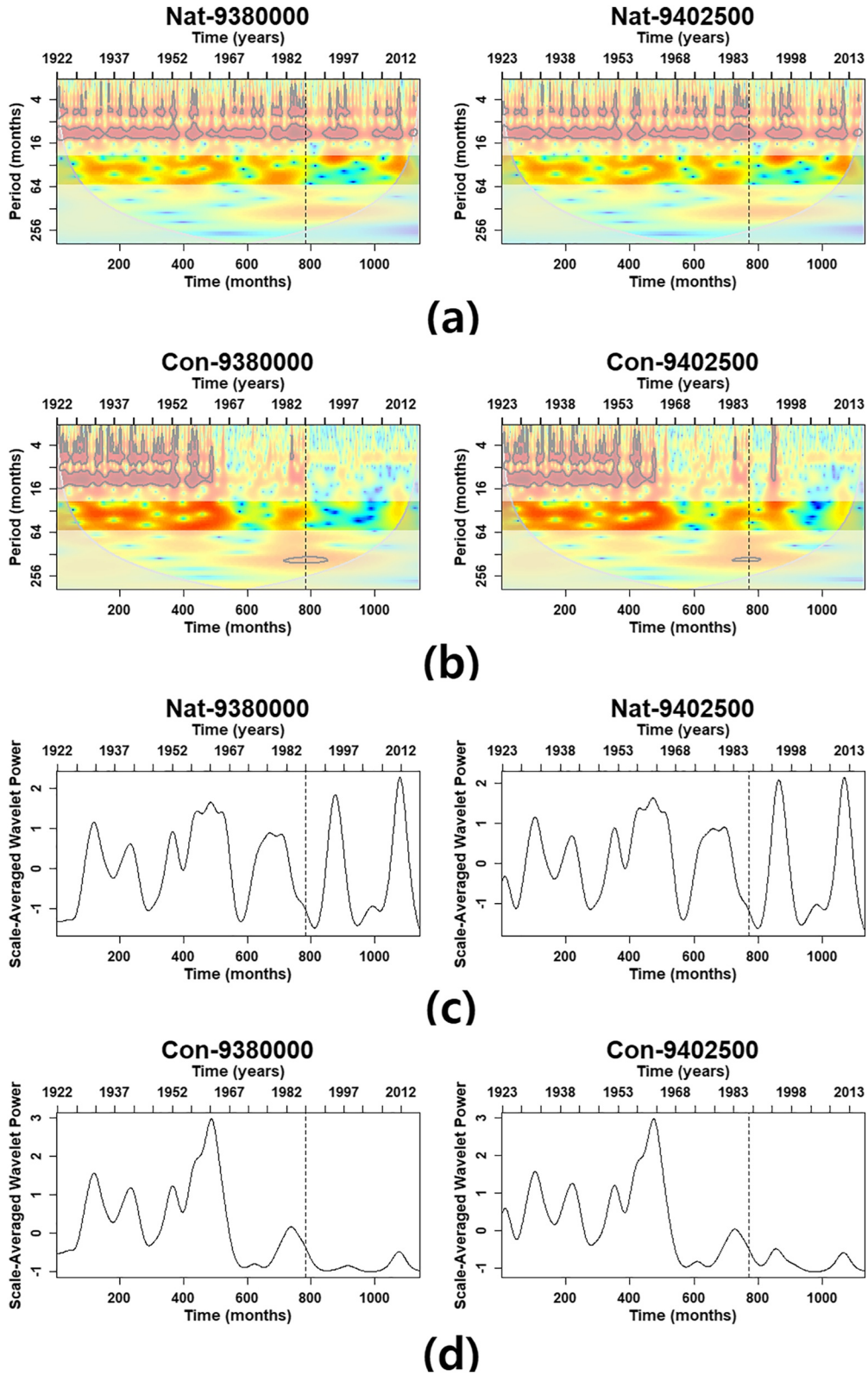

Figure A6. Wavelet power spectrum of the naturalized streamflow (a) and the controlled streamflow (b) at stations of Cluster-4 from the multi-annual frequency analysis. The scale-averaged wavelet power is also presented for both naturalized flow (c) and controlled flow (d) at these stations.

Data Availability Statement

Observed flow data may be obtained from U.S. Geological Survey (2020): Available at <http://waterdata.usgs.gov/nwis/>. NWIS Site Numbers are available in Table 1. Naturalized flow data may be obtained from U.S. Bureau of Reclamation (2020): Available at <https://www.usbr.gov/lc/region/g4000/NaturalFlow/NaturalFlows1906-2018_20200110.xlsx>. Dams data may be obtained from U.S. Army Corps of Engineers (2020): Available at <https://nid.sec.usace.army.mil/ords/f?p=105:19:12463373659661::NO:::>. The data files corresponding to AZ, CA, CO, NM, NV, UT, WY were used in this study.

Acknowledgments
This work was supported by the United States Geological Survey (USGS) Powell Center Working Group Project "A global synthesis of land surface fluxes under natural and human-altered watersheds using the Budyko framework". Support for Jeongwoo Hwang and Naresh Devineni is provided by the U.S. Department of Energy Early CAREER Award No. DE-SC0018124.

References

Bain, M. B., Finn, J. T., & Booke, H. E. (1988). Streamflow regulation and fish community structure. *Ecology*, *69*(2), 382–392. https://doi.org/10.2307/1940436
Berndt, D. J., & Clifford, J. (1994). Using dynamic time warping to find patterns in time series. *KDD workshop*, *10*(16), 359–370.
Box, G. E. P., & Jenkins, G. M. (1970). *Time series analysis: Forecasting and control*. San Francisco: Holden-Day.
Brandt, S. A. (2000). Classification of geomorphological effects downstream of dams. *Catena*, *40*(4), 375–401. https://doi.org/10.1016/s0341-8162(00)00093-x
Bruce, B. W. (2012). *WaterSMART—The Colorado River Basin focus area study*. Washington DC, USA: US Geological Survey.
Bunn, S. E., & Arthington, A. H. (2002). Basic principles and ecological consequences of altered flow regimes for aquatic biodiversity. *Environmental Management*, *30*(4), 492–507. https://doi.org/10.1007/s00267-002-2737-0
Chalise, D. R., Sankarasubramanian, A., & Ruhi, A. (2021). Dams and climate interact to alter river flow regimes across the United States. *Earth's Future*, *9*(4), e2020EF001816. https://doi.org/10.1029/2020ef001816
Christensen, N. S., Wood, A. W., Voisin, N., Lettenmaier, D. P., & Palmer, R. N. (2004). The effects of climate change on the hydrology and water resources of the Colorado River basin. *Climatic Change*, *62*(1), 337–363. https://doi.org/10.1023/b:clim.0000013684.13621.1f
Ciria, T. P., Labat, D., & Chiogna, G. (2019). Detection and interpretation of recent and historical streamflow alterations caused by river damming and hydropower production in the Adige and Inn river basins using continuous, discrete and multiresolution wavelet analysis. *Journal of Hydrology*, *578*, 124021. https://doi.org/10.1016/j.jhydrol.2019.124021
Comte, L., Grantham, T., & Ruhi, A. (2021). Human stabilization of river flows is linked with fish invasions across the USA. *Global Ecology and Biogeography*, *30*(3), 725–737. https://doi.org/10.1111/geb.13258
Couto, T. B., & Olden, J. D. (2018). Global proliferation of small hydropower plants–science and policy. *Frontiers in Ecology and the Environment*, *16*(2), 91–100. https://doi.org/10.1002/fee.1746
Douglas, M. W., Maddox, R. A., Howard, K., & Reyes, S. (1993). The Mexican monsoon. *Journal of Climate*, *6*(8), 1665–1677. https://doi.org/10.1175/1520-0442(1993)006<1665:TMM>2.0.CO;2
Farge, M. (1992). Wavelet transforms and their applications to turbulence. *Annual Review of Fluid Mechanics*, *24*(1), 395–458. https://doi.org/10.1146/annurev.fl.24.010192.002143
Foufoula-Georgiou, E., & Kumar, P. (Eds.). (2014). *Wavelets in geophysics*. Elsevier.
Gao, Y., Vogel, R. M., Kroll, C. N., Poff, N. L., & Olden, J. D. (2009). Development of representative indicators of hydrologic alteration. *Journal of Hydrology*, *374*(1–2), 136–147. https://doi.org/10.1016/j.jhydrol.2009.06.009
Graf, W. L. (1999). Dam nation: A geographic census of American dams and their large-scale hydrologic impacts. *Water Resources Research*, *35*(4), 1305–1311. https://doi.org/10.1029/1999wr900016
Graf, W. L. (2006). Downstream hydrologic and geomorphic effects of large dams on American rivers. *Geomorphology*, *79*(3–4), 336–360. https://doi.org/10.1016/j.geomorph.2006.06.022
Grill, G., Dallaire, C. O., Chouinard, E. F., Sindorf, N., & Lehner, B. (2014). Development of new indicators to evaluate river fragmentation and flow regulation at large scales: A case study for the Mekong River Basin. *Ecological Indicators*, *45*, 148–159. https://doi.org/10.1016/j.ecolind.2014.03.026
Grill, G., Lehner, B., Lumsdon, A. E., MacDonald, G. K., Zarfl, C., & Liermann, C. R. (2015). An index-based framework for assessing patterns and trends in river fragmentation and flow regulation by global dams at multiple scales. *Environmental Research Letters*, *10*(1), 015001. https://doi.org/10.1088/1748-9326/10/1/015001
Grinsted, A., Moore, J. C., & Jevrejeva, S. (2004). Application of the cross wavelet transform and wavelet coherence to geophysical time series. *Nonlinear Processes in Geophysics*, *11*(5/6), 561–566. https://doi.org/10.5194/npg-11-561-2004
Hidalgo, H. G., & Dracup, J. A. (2003). ENSO and PDO effects on hydroclimatic variations of the Upper Colorado River Basin. *Journal of Hydrometeorology*, *4*(1), 5–23. https://doi.org/10.1175/1525-7541(2003)004<0005:EAPEOH>2.0.CO;2
Higgins, R. W., Chen, Y., & Douglas, A. V. (1999). Interannual variability of the North American warm season precipitation regime. *Journal of Climate*, *12*(3), 653–680. https://doi.org/10.1175/1520-0442(1999)012<0653:IVOTNA>2.0.CO;2
Hubbard, B. B. (1996). *The world according to wavelets the story of a mathematical technique in the making*. Universities Press.
Kalra, A., & Ahmad, S. (2012). Estimating annual precipitation for the Colorado River Basin using oceanic-atmospheric oscillations. *Water Resources Research*, *48*. https://doi.org/10.1029/2011wr010667
Kendall, M. G. (1948). *Rank correlation methods*. Griffin.
Kennedy, T. A., Muehlbauer, J. D., Yackulic, C. B., Lytle, D. A., Miller, S. W., Dibble, K. L., et al. (2016). Flow management for hydropower extirpates aquatic insects, undermining river food webs. *BioScience*, *66*(7), 561–575. https://doi.org/10.1093/biosci/biw059
Keogh, E., & Ratanamahatana, C. A. (2005). Exact indexing of dynamic time warping. *Knowledge and Information Systems*, *7*(3), 358–386. https://doi.org/10.1007/s10115-004-0154-9
Koch, F., Prasch, M., Bach, H., Mauser, W., Appel, F., & Weber, M. (2011). How will hydroelectric power generation develop under climate change scenarios? A case study in the Upper Danube basin. *Energies*, *4*(10), 1508–1541. https://doi.org/10.3390/en4101508
Kulkarni, J. R. (2000). Wavelet analysis of the association between the southern oscillation and the Indian summer monsoon. *International Journal of Climatology: A Journal of the Royal Meteorological Society*, *20*(1), 89–104. https://doi.org/10.1002/(sici)1097-0088(200001)20:1<89::AID-JOC458>3.0.CO;2-W
Kumar, P., & Foufoula-Georgiou, E. (1997). Wavelet analysis for geophysical applications. *Reviews of Geophysics*, *35*(4), 385–412. https://doi.org/10.1029/97rg00427

Kwon, H. H., Lall, U., & Khalil, A. F. (2007). Stochastic simulation model for nonstationary time series using an autoregressive wavelet decomposition: Applications to rainfall and temperature. *Water Resources Research*, *43*. https://doi.org/10.1029/2006wr005258
Kwon, H. H., Lall, U., Moon, Y. I., Khalil, A. F., & Ahn, H. (2006). Episodic interannual climate oscillations and their influence on seasonal rainfall in the Everglades National Park. *Water Resources Research*, *42*. https://doi.org/10.1029/2006wr005017
Labat, D. (2005). Recent advances in wavelet analyses: Part 1. A review of concepts. *Journal of Hydrology*, *314*(1–4), 275–288. https://doi.org/10.1016/j.jhydrol.2005.04.003
Lehner, B., Liermann, C. R., Revenga, C., Vörösmarty, C., Fekete, B., Crouzet, P., et al. (2011). High-resolution mapping of the world's reservoirs and dams for sustainable river-flow management. *Frontiers in Ecology and the Environment*, *9*(9), 494–502. https://doi.org/10.1890/100125
Lytle, D. A., & Poff, N. L. (2004). Adaptation to natural flow regimes. *Trends in Ecology & Evolution*, *19*(2), 94–100. https://doi.org/10.1016/j.tree.2003.10.002
Mailhot, A., Talbot, G., Ricard, S., Turcotte, R., & Guinard, K. (2018). Assessing the potential impacts of dam operation on daily flow at ungauged river reaches. *Journal of Hydrology: Regional Studies*, *18*, 156–167. https://doi.org/10.1016/j.ejrh.2018.06.006
Mann, H. B. (1945). Nonparametric tests against trend. *Econometrica: Journal of the econometric society*, *13*, 245–259. https://doi.org/10.2307/1907187
Maupin, M. A., Ivahnenko, T. I., & Bruce, B. (2018). *Estimates of water use and trends in the Colorado River Basin, Southwestern United States, 1985–2010 (No. 2018-5049)*. US Geological Survey.
Milly, P. C. D., & Wetherald, R. T. (2002). Macroscale water fluxes 3. Effects of land processes on variability of monthly river discharge. *Water Resources Research*, *38*(11), 17–1. https://doi.org/10.1029/2001wr000761
Mukhopadhyay, S., Sankarasubramanian, A., & Awasthi, C. (2020). Developing the hydrological dependency structure between stream-gage and reservoir networks. *Scientific Data*, *7*(1), 1–9. https://doi.org/10.1038/s41597-020-00660-6
National Research Council. (1992). *Restoration of aquatic ecosystems: Science, technology, and public policy*. National Academies Press.
Nilsson, C., Reidy, C. A., Dynesius, M., & Revenga, C. (2005). Fragmentation and flow regulation of the world's large river systems. *Science*, *308*(5720), 405–408. https://doi.org/10.1126/science.1107887
Nowak, K., Hoerling, M., Rajagopalan, B., & Zagona, E. (2012). Colorado River basin hydroclimatic variability. *Journal of Climate*, *25*(12), 4389–4403. https://doi.org/10.1175/jcli-d-11-00406.1
Olden, J. D., & Naiman, R. J. (2010). Incorporating thermal regimes into environmental flows assessments: Modifying dam operations to restore freshwater ecosystem integrity. *Freshwater Biology*, *55*(1), 86–107. https://doi.org/10.1111/j.1365-2427.2009.02179.x
Palmer, M., & Ruhi, A. (2019). Linkages between flow regime, biota, and ecosystem processes: Implications for river restoration. *Science*, *365*(6459). https://doi.org/10.1126/science.aaw2087
Patskoski, J., Sankarasubramanian, A., & Wang, H. (2015). Reconstructed streamflow using SST and tree-ring chronologies over the southeastern United States. *Journal of Hydrology*, *527*, 761–775. https://doi.org/10.1016/j.jhydrol.2015.05.041
Poff, N. L. (2018). Beyond the natural flow regime? Broadening the hydro-ecological foundation to meet environmental flows challenges in a non-stationary world. *Freshwater Biology*, *63*(8), 1011–1021. https://doi.org/10.1111/fwb.13038
Poff, N. L., Olden, J. D., Merritt, D. M., & Pepin, D. M. (2007). Homogenization of regional river dynamics by dams and global biodiversity implications. *Proceedings of the National Academy of Sciences*, *104*(14), 5732–5737. https://doi.org/10.1073/pnas.0609812104
Poff, N. L., Richter, B. D., Arthington, A. H., Bunn, S. E., Naiman, R. J., Kendy, E., et al. (2010). The ecological limits of hydrologic alteration (ELOHA): A new framework for developing regional environmental flow standards. *Freshwater Biology*, *55*(1), 147–170. https://doi.org/10.1111/j.1365-2427.2009.02204.x
Prairie, J., & Callejo, R. (2005). Natural flow and salt computation methods, Calendar Years 1971–1995 (Vol. 135). All US Government Documents (Utah Regional Depository).
Redmond, K. T., & Koch, R. W. (1991). Surface climate and streamflow variability in the western United States and their relationship to large-scale circulation indices. *Water Resources Research*, *27*(9), 2381–2399. https://doi.org/10.1029/91wr00690
Richter, B. D., Baumgartner, J. V., Powell, J., & Braun, D. P. (1996). A method for assessing hydrologic alteration within ecosystems. *Conservation Biology*, *10*(4), 1163–1174. https://doi.org/10.1046/j.1523-1739.1996.10041163.x
Richter, B. D., & Thomas, G. A. (2007). Restoring environmental flows by modifying dam operations. *Ecology and Society*, *12*(1). https://doi.org/10.5751/es-02014-120112
Ripl, W. (2003). Water: The bloodstream of the biosphere. *Philosophical Transactions of the Royal Society of London. Series B: Biological Sciences*, *358*(1440), 1921–1934. https://doi.org/10.1098/rstb.2003.1378
Ropelewski, C. F., & Halpert, M. S. (1986). North American precipitation and temperature patterns associated with the El Niño/Southern Oscillation (ENSO). *Monthly Weather Review*, *114*(12), 2352–2362. https://doi.org/10.1175/1520-0493(1986)114<2352:NAPATP>2.0.CO;2
Ruhi, A., Dong, X., McDaniel, C. H., Batzer, D. P., & Sabo, J. L. (2018). Detrimental effects of a novel flow regime on the functional trajectory of an aquatic invertebrate metacommunity. *Global Change Biology*, *24*(8), 3749–3765. https://doi.org/10.1111/gcb.14133
Ruhi, A., Hwang, J., Devineni, N., Mukhopadhyay, S., Kumar, H., Comte, L., et al. (2019). How does flow alteration propagate across a large, highly-regulated basin? Dam attributes, network context, and implications for biodiversity. In *AGU Fall Meeting Abstracts* (p. H23N-2086).
Sheppard, P. R., Comrie, A. C., Packin, G. D., Angersbach, K., & Hughes, M. K. (2002). The climate of the US Southwest. *Climate Research*, *21*(3), 219–238. https://doi.org/10.3354/cr021219
Sivapalan, M., Takeuchi, K., Franks, S. W., Gupta, V. K., Karambiri, H., Lakshmi, V., et al. (2003). IAHS Decade on Predictions in Ungauged Basins (PUB), 2003–2012: Shaping an exciting future for the hydrological sciences. *Hydrological Sciences Journal*, *48*(6), 857–880. https://doi.org/10.1623/hysj.48.6.857.51421
Snyder, F. F. (1964). Hydrology of spillway design: Large structures-adequate data. *Journal of the Hydraulics Division*, *90*(3), 239–259. https://doi.org/10.1061/jyceaj.0001045
Tamaddun, K. A., Kalra, A., & Ahmad, S. (2017). Wavelet analyses of western US streamflow with ENSO and PDO. *Journal of Water and Climate Change*, *8*(1), 26–39. https://doi.org/10.2166/wcc.2016.162
Terrier, M., Perrin, C., De Lavenne, A., Andréassian, V., Lerat, J., & Vaze, J. (2021). Streamflow naturalization methods: A review. *Hydrological Sciences Journal*, *66*(1), 12–36. https://doi.org/10.1080/02626667.2020.1839080
Thomas, H. A., & Fiering, M. (1962). Mathematical synthesis of stream flow sequences for the analysis of river basins by simulation, Ch. 12. In A. Maass (Ed.), *Design of water resource systems*. Harvard University Press.
Thorndike, R. L. (1953). Who belongs in the family? *Psychometrika*, *18*(4), 267–276. https://doi.org/10.1007/bf02289263
Topping, D. J., Rubin, D. M., & Vierra, L. E., Jr (2000). Colorado River sediment transport: 1. Natural sediment supply limitation and the influence of Glen Canyon Dam. *Water Resources Research*, *36*(2), 515–542. https://doi.org/10.1029/1999wr900285

Torrence, C., & Compo, G. P. (1998). A practical guide to wavelet analysis. *Bulletin of the American Meteorological Society*, *79*(1), 61–78. https://doi.org/10.1175/1520-0477(1998)079<0061:APGTWA>2.0.CO;2

Torrence, C., & Webster, P. J. (1999). Interdecadal changes in the ENSO–monsoon system. *Journal of Climate*, *12*(8), 2679–2690. https://doi.org/10.1175/1520-0442(1999)012<2679:ICITEM>2.0.CO;2

U.S. Army Corps of Engineers. (2020). *National Inventory of Dams*, Washington D. C. accessed March 2020. Retrieved from https://nid.sec.usace.army.mil/ords/f?p=105:19:12463373659661.::NO:::

U.S. Bureau of Reclamation. (1922). *Colorado River Compact, 1922*. accessed June 2021. Retrieved from https://www.usbr.gov/lc/region/pao/pdfiles/crcompct.pdf

U.S. Bureau of Reclamation. (1946). Utilization of Waters of Colorado and Tijuana Rivers and of the Rio Grande: Treaty between the United States of America and Mexico. accessed January 2021. Retrieved from https://www.usbr.gov/lc/region/pao/pdfiles/mextrety.pdf

U.S. Bureau of Reclamation. (2020). Colorado River Basin Natural Flow and Salt Data. accessed March 2020. Retrieved from https://www.usbr.gov/lc/region/g4000/NaturalFlow/NaturalFlows1906-2018_20200110.xlsx

U.S. Department of the Interior and Office of the Secretary of the Interior. (1996). *Appendix G, record of decision, operation of Glen Canyon Dam: Final environmental impact statement*. accessed July 2021. Retrieved from https://www.usbr.gov/uc/envdocs/rod/Oct1996_OperationGCD_ROD.pdf

U. S. Fish and Wildlife Service. (1991). *Final biological opinion for the Animas-La Plata Project, Colorado and New Mexico*. Denver, CO: Fish and Wildlife Service.

U. S. Fish and Wildlife Service. (1992). *Final biological opinion on the operation of Flaming Gorge DamFish and Wildlife Service*. Denver, CO: Mountain-Prairie Region.

U.S. Geological Survey. (2020). *National Water Information System data available on the World Wide Web (USGS Water Data for the Nation)*, accessed March 2020. Retrieved from http://waterdata.usgs.gov/nwis/

Vogel, R. M., Lall, U., Cai, X., Rajagopalan, B., Weiskel, P. K., Hooper, R. P., & Matalas, N. C. (2015). Hydrology: The interdisciplinary science of water. *Water Resources Research*, *51*, 4409–4430. https://doi.org/10.1002/2015wr017049

Vörösmarty, C. J., & Sahagian, D. (2000). Anthropogenic disturbance of the terrestrial water cycle. *BioScience*, *50*(9), 753–765. https://doi.org/10.1641/0006-3568(2000)050[0753:ADOTTW]2.0.CO;2

Vörösmarty, C. J., Sharma, K. P., Fekete, B. M., Copeland, A. H., Holden, J., Marble, J., & Lough, J. A. (1997). *The storage and aging of continental runoff in large reservoir systems of the world*. Ambio (Sweden).

Wang, B., & Wang, Y. (1996). Temporal structure of the Southern Oscillation as revealed by waveform and wavelet analysis. *Journal of Climate*, *9*(7), 1586–1598. https://doi.org/10.1175/1520-0442(1996)009<1586:tsotso>2.0.co;2

Wang, H., Brill, E. D., Ranjithan, R. S., & Sankarasubramanian, A. (2015). A framework for incorporating ecological releases in single reservoir operation. *Advances in Water Resources*, *78*, 9–21. https://doi.org/10.1016/j.advwatres.2015.01.006

Webb, R. H., & Betancourt, J. L. (1992). *Climatic variability and flood frequency of the Santa Cruz River, Pima County, Arizona (No. 2379)*. US Geological Survey.

Weng, H., & Lau, K. M. (1994). Wavelets, period doubling, and time–frequency localization with application to organization of convection over the tropical western Pacific. *Journal of the Atmospheric Sciences*, *51*(17), 2523–2541. https://doi.org/10.1175/1520-0469(1994)051<2523:WPDATL>2.0.CO;2

White, M. A., Schmidt, J. C., & Topping, D. J. (2005). Application of wavelet analysis for monitoring the hydrologic effects of dam operation: Glen Canyon Dam and the Colorado River at Lees Ferry, Arizona. *River Research and Applications*, *21*(5), 551–565. https://doi.org/10.1002/rra.827

Whitlock, C., & Bartlein, P. J. (1993). Spatial variations of Holocene climatic change in the Yellowstone region. *Quaternary Research*, *39*(2), 231–238. https://doi.org/10.1006/qres.1993.1026

Wiele, S. M., & Smith, J. D. (1996). A reach-averaged model of diurnal discharge wave propagation down the Colorado River through the Grand Canyon. *Water Resources Research*, *32*(5), 1375–1386. https://doi.org/10.1029/96wr00199

Willis, C. M., & Griggs, G. B. (2003). Reductions in fluvial sediment discharge by coastal dams in California and implications for beach sustainability. *The Journal of Geology*, *111*(2), 167–182. https://doi.org/10.1086/345922

Yang, Y. C. E., & Cai, X. (2011). Reservoir reoperation for fish ecosystem restoration using daily inflows—Case study of Lake Shelbyville. *Journal of Water Resources Planning and Management*, *137*(6), 470–480. https://doi.org/10.1061/(asce)wr.1943-5452.0000139